



Surface ozone (O₃) pollution is assessed across Ireland with a focus on long-term trends with a specific focus on the Mace Head atmospheric research station which monitors background O₃ advected into Europe via prevailing South Westerlies. Using innovative trajectory analysis, O₃ concentrations, exceedances and were identified by sectors, revealing distinct seasonal and spatial patterns. Findings show a significant rising trend in surface O₃ at Irish urban sites over the past two decades but without a similar trend at coastal sites. Highest O₃ levels and exceedances were observed at remote coastal sites, less influenced by local emissions, and heavily influenced by meteorological processes, including transboundary pollution and stratospheric intrusion. At Mace Head, springtime O₃ levels show a declining trend, with a



25 rising winter-time trend. Looking only at the clean sector, the springtime decline remains
26 significant; but without rising wintertime trends, implying the rising winter trends are a
27 response to declining European emissions. Advanced modelling tools are used to quantify O₃
28 source contributions, elucidating key drivers behind the observed changes. Characteristic
29 springtime O₃ maxima at Mace Head are attributed to stratospheric transport, influences from
30 westerly transboundary air pollution, and lightning NO_x. Combined trend and sectoral
31 observational analysis reveals that total spring-time concentrations are in decline, with
32 exceedances from the UK & continental sector declining at a greater rate. This research
33 highlights the importance of seasonal factors in air quality management across Ireland,
34 emphasising the need for a multi-faceted approach to control O₃ levels and reduce exceedances
35 through global and regional emission reductions.

36 **Keywords** - Meteorology, NO_x, Climate, CH₄, Emissions, VOC.

37 **1. Introduction**

38 Surface Ozone (O₃) has significant implications for health, vegetation, and climate. As O₃ is
39 highly reactive, its chemical production is driven by complex photochemical processes,
40 responding non-linearly to pollution control, creating challenges for its effective regulation.
41 Elevated O₃ levels cause severe health issues, prolonged exposure to high O₃ levels is linked
42 to respiratory issues, cardiovascular problems, and reduced lung function, particularly in
43 sensitive populations such as children, the elderly, and individuals with pre-existing respiratory
44 conditions (Lin et al., 2018; Todorović et al., 2019; Zhang et al., 2019, WHO, 2021). O₃
45 pollution can adversely impact vegetation by reducing agricultural productivity (Ashmore et
46 al., 2005; Paoletti et al., 2006). O₃ is also the third most significant greenhouse gas after Carbon
47 Dioxide (CO₂) and methane (CH₄), contributing to climate instability (IPCC, 2021). The
48 lifetime of O₃ in the free troposphere is on the order of several weeks, and it is affected by



49 large-scale atmospheric circulation patterns (Wespes et al., 2017), and meteorological factors
50 such as temperature, solar radiation, wind speed, and atmospheric stability play a significant
51 role in O₃ formation. (Ding et al., 2023; Khiem et al., 2010).

52 O₃ is formed in the atmosphere from precursors Nitrogen Oxides (NO_x), carbon monoxide
53 (CO), and volatile organic compounds (VOCs) through photochemical reactions. The reactive,
54 interdependent atmospheric chemistry leads to a non-linear relationship between O₃ and its
55 precursors (Seinfeld and Pandis, 2016), and effective O₃ mitigation requires an understanding
56 of processes influencing O₃ production and removal mechanisms (Fowler et al., 2013). NO_x
57 can suppress or enhance O₃ formation, depending on the atmospheric chemistry regime. In
58 polluted urban environments, high NO_x emissions can lead to O₃ dissociation, retarding
59 formation whereas in relatively clean environments, O₃ formation is correlated with NO_x
60 concentration (Seinfeld and Pandis, 1997; Tavella & da Silva Júnior, 2021). Seasonal and
61 regional variations further complicate the regulation, with higher O₃ levels observed in summer
62 across the northern hemisphere due to increased temperatures, solar radiation, and abundant
63 precursors (Moiseenko et al., 2021; Sicard et al., 2016). In marine boundary layers, O₃ levels
64 are generally lower than in continental regions, though specific oceanic environments can
65 exhibit high O₃ concentrations due to inflows from polluted areas (Boylan et al., 2014; Girach
66 et al., 2020). Another factor which influences O₃ level is the North Atlantic Oscillation (NAO
67 which influences O₃ levels in Western Europe, with positive phases enhancing the transport of
68 O₃ and precursors from North America. This effect is particularly notable in southwest, central,
69 and northern Europe (Bonaccorso et al., 2015; Creilson et al., 2003; Pausata et al., 2012).
70 While Ireland's air quality is mostly governed by the influx of clean maritime air from the
71 Atlantic Ocean (Tripathi et al., 2010), particular synoptic scenarios allow for the intrusion of
72 polluted air masses from continental Europe. These events, though infrequent, can bring



73 substantial amounts of ozone and its precursors (NO_x , VOCs), contributing to short-term O_3
74 pollution episodes.

75 The World Health Organisation (WHO) publishes Air Quality Guidelines (AQGs) as a non-
76 legally binding global target for governments to achieve within their jurisdictions. These AQGs
77 comprise evidence-based recommendations of limit values to protect public health. The current
78 recommended AQGs for O_3 is expressed as a daily maximum of 8-hourly running average O_3
79 value of $100 \mu\text{g}/\text{m}^3$. Days when O_3 levels exceed the recommended AQGs are classified as
80 exceedance days. Factors contributing to exceedances include high solar radiation, stagnant air
81 masses, and local emissions and regional and transboundary transport of O_3 and precursors.

82 Over the past 150 years, there has been a 40% increase in O_3 levels owing to rising precursor
83 emissions. (Archibald et al., 2020; Griffiths et al., 2021; Young et al., 2013). Despite European
84 Union emission reduction policies, O_3 pollution remains a problem, with over 94% of those
85 living in European cities exposed to O_3 levels exceeding the WHO AQGs in 2022 (EEA 2024,
86 WHO 2021). Over 22,000 premature deaths in the EU were attributable to short-term exposure
87 to O_3 in 2021 (Soares et al., 2023).

88 Long-term data from the Mace Head research station in Ireland reveal seasonal peaks in O_3
89 during spring and lows in summer. (Derwent, 1998; Derwent et al., 1994, 2018a). Historical
90 trends show increasing baseline O_3 levels in the 1980s and 1990s, stability in the 2000s, and a
91 decline in the 2010s. (Derwent et al., 2013; Derwent, Manning, Simmonds, Spain, et al., 2018).
92 Recent observational and modelling data have identified a broad O_3 maximum in spring and
93 early summer, aligning with peak stratospheric transport (Ansari et al., 2024; Lin et al., 2012;
94 Russo et al., 2023). O_3 dynamics are complex, and studies reveal discrepancies between model
95 output and observations (Bessagnet et al., 2016; Vautard et al., 2012), highlighting the need for
96 further understanding of factors governing O_3 levels and trends.



97 This study investigates the distribution and trends of O₃ and its precursors across Ireland,
98 providing valuable insights into the regional and hemispheric impact on Irish surface O₃ levels
99 and exceedances. By analysing a long term observational dataset, this research highlights
100 significant seasonal and temporal variations and long-term trends in O₃ concentrations.
101 Advanced modelling results using the Tropospheric Ozone Attribution of Sources with Tagging
102 1.0 (TOAST 1.0) framework (Butler et al., 2018; Butler et al., 2020) were applied to determine
103 the drivers of O₃ trends in Ireland. Additionally, trajectory analysis is used to trace the origins
104 of air masses, revealing the impact of transboundary pollution and atmospheric transport. This
105 integrated approach not only enhances our understanding of the drivers of O₃ concentrations,
106 trends and exceedances over Ireland but also underscores the importance of global and regional
107 contributions to O₃.

108 **2. Data and methodology**

109 **2.1 Observational Network and Analysis Approach**

110 Measurement data is obtained from the Environmental Protection Agency, Ireland (EPA)
111 (<https://eparesearch.epa.ie/safer/>). The O₃ monitoring network shown in Figure 1 has been
112 operational in Ireland since 1994. O₃ is measured using an API M400 and O₃ analyser based
113 on UV photometry at all monitoring sites. Measurements of O₃ precursors from EPA air quality
114 monitoring sites are also monitored. The details of measurements site are shown in table 1 .
115 Numerous previous studies have analysed this data, with a particular focus on the analysis of
116 Mace Head data to assess background levels of (Carslaw, 2005; Derwent, 1998; Derwent et al.,
117 1994, 1998, 2001, 2004, 2008, 2013; Derwent, Manning, Simmonds, & Doherty, 2018;
118 Derwent, Manning, Simmonds, Spain, et al., 2018; Oltmans et al., 2013; Simmonds et al., 2004;
119 O. P. Tripathi et al., n.d., 2010, 2012, 2013). Additionally, the CH₄ data is obtained from the

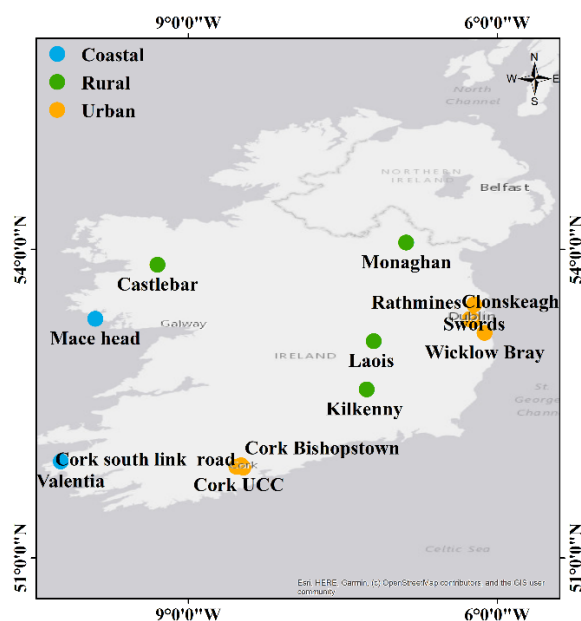


120 Integrated Carbon Observation System (ICOS) network, accessible at <https://www.icos->
121 [cp.eu/data-products/ATM_NRT_CO2_CH4](https://www.icos-cp.eu/data-products/ATM_NRT_CO2_CH4).

122 For this analysis, the observational sites were classified into three categories: Coastal, Rural,
123 and Urban, as shown in Figure 1. The classification of the sites is based on Spohn et al., 2022,
124 with the addition of the coastal category. Hourly data were used to evaluate annual trends based
125 on monthly mean concentrations. Seasonal analysis conducted for the four main
126 meteorological seasons in Ireland, namely Spring (March, April, May), Summer (June, July,
127 August), Autumn (September, October, November), and Winter (December, January,
128 February). O₃ exceedances were calculated based on the WHO AQGs, indicating that the
129 maximum daily average over eight hours (MDA8) should not exceed 100 µg/m³. A significant
130 analysis was performed on data measured at the Mace Head Atmospheric Research Station
131 (53°33'N, 9°54' W), which is exposed to pristine marine air masses approximately half of the
132 time. (Grigas et al., 2017; O'Dowd et al., 2014).

133 **Table 1.** Details of Environmental Protection Agency Ireland (EPA) O₃ measurement sites over
134 Ireland, with location information, and the data period used for the study.

Site	Data availability	Type	Latitude	Longitude
Mace head	1994-2022	Coastal	53.3253	-9.9036
Valentia	2001-2022	Coastal	51.9385	-10.24
Monaghan	1995-2022	Rural	54.0661	-6.883
Laois	2005-2022	Rural	53.1076	-7.1983
Kilkenny	2012-2022	Rural	52.6383	-7.2676
Rathmines	2002-2022	Urban	53.322	-6.2672
Clonskeagh	2008-2022	Urban	53.3118	-6.2353
Mayo Castlebar	2009-2022	Urban	53.851	-9.3003
Swords	2009-2022	Urban	53.4631	-6.2222
Wicklow Bray	2009-2022	Urban	53.1873	-6.122
Cork South link road	2014-2022	Urban	51.8785	-8.4649
Cork Bishops town	2016-2022	Urban	51.8858	-8.53321
Cork UCC	2018-2022	Urban	51.9	-8.4863



135

136

137

138

139 **Figure 1.** – The map of EPA O₃ measurement sites over Ireland with classification of
140 backgrounds.

141 Trend analysis was conducted using the Openair package in R. This software tool is designed
142 for the analysis of atmospheric composition data. Trends were determined using the Theil-Sen
143 slope estimator and Mann-Kendall tests to quantify significance, in accordance with the
144 Tropospheric Ozone Assessment Report (TOAR) guidelines (Lefohn et al., 2018). It is a robust
145 method for estimating trend slopes in time series data, preferable to traditional least-squares
146 regression, which can be sensitive to extreme values and outliers. Uncertainty or reliability of
147 the trend is calibrated according to the p-value, as outlined by (Chang et al., 2023), consistent
148 with the best statistical practices for analysis used in the second phase of TOAR.



149 **2.2 Clean air sector identification from Back trajectories**

150 Baseline O₃ refers to the concentration of O₃ in air masses minimally influenced by local or
151 regional anthropogenic emissions. Back-trajectory methods are widely used to estimate
152 baseline O₃ levels by analysing the origins and transport pathways of air masses reaching
153 observation sites. Typically, Lagrangian dispersion models are used to trace air parcels
154 backwards in time and identify their origin.

155 For this study, air mass trajectories arriving at Mace Head were calculated using the Hybrid
156 Single Particle Lagrangian Integrated Trajectory Model (HYSPLIT) (Draxler et al., 2003; Stein
157 et al., 2015) in conjunction with R software. The air masses were classified into two categories
158 the clean sector and EU-influenced sector. An air mass was considered part of the clean sector
159 consider when air mass trajectories remained over the ocean surface for the previous 72 hours.
160 And the remaining air mass trajectories are classified as the EU-influenced sector.
161 Meteorological data for the analysis were derived from NOAA reanalysis data (Stunder et al.,
162 2004). Calculations were performed for 6:00 UTC each day, with a final trajectory height of
163 100 meters, covering the years 2000 to 2022. The O₃ concentrations observed during the clean
164 sector were averaged to derive baseline levels, consistent with previous studies on baseline O₃
165 trends and sources (Derwent et al., 2013; Oltmans et al., 2006).

166

167 **2.3 CAM4-Chem Model**

168 The CAM-Chem air quality model, part of the Community Earth System Model (CESM),
169 simulates atmospheric chemistry and the interactions among chemical constituents,
170 meteorology, and climate. It incorporates detailed chemical mechanisms, emission inventories,
171 and meteorological data to simulate pollutant dispersion, thereby allowing us to determine air
172 quality trends. CAM-Chem has been applied in numerous studies, significantly contributing to



173 the understanding of regional and global atmospheric processes. (Lamarque et al., 2012; Tilmes
174 et al., 2016). The model features a flexible chemical pre-processor to allow for detailed
175 handling of atmospheric chemistry. Studies have demonstrated that CAM-Chem accurately
176 represents conditions in both the troposphere. (Aghedo et al., 2011; Lamarque et al., 2010) and
177 the stratosphere (Lamarque et al., 2008; Lamarque and Solomon, 2010), including temperature
178 structure and dynamics (Butchart et al., 2011). Offline CAM-Chem has also been utilised in
179 the Hemispheric Transport of Air Pollution (HTAP) assessments. (Anenberg et al., 2009; Fiore
180 et al., 2009; Jonson et al., 2010; Shindell et al., 2008; Tan et al., 2018).

181 For the current study, we analyse simulations of the Community Atmospheric Model version 4
182 CAM4-Chem (Community Atmosphere Model version 4 with chemistry) ((Lamarque et al.,
183 2012). The model simulations were carried out at a horizontal resolution of $1.9^{\circ} \times 2.5^{\circ}$,
184 featuring 56 vertical levels for the 2000-2018 period, with specified dynamics derived from
185 MERRA2 reanalysis. (Molod et al., 2015). Tagged source attribution of tropospheric
186 ozone (TOAST 1.0) is a novel tagging methodology developed for the CESM to quantify
187 source contributions to O_3 . Unlike traditional methods that rely on sensitivity simulations,
188 TOAST uses an online tagging approach to track O_3 production from specific NO_x and VOC
189 sources (e.g., anthropogenic, biogenic, biomass burning, lightning) directly within the model,
190 allowing for efficient attribution of O_3 to regional and sectoral emissions while maintaining
191 full chemical coupling. The tool has been validated against observations and demonstrates
192 utility in disentangling the impacts of different emission sectors on O_3 pollution. (Butler et al.,
193 2018, 2020; Lupaşcu et al., 2022; Nalam et al., 2024)

194 Global CAM4-Chem model simulations are performed for the years 2000-2018 with NO_x and
195 VOC tagging (as described in Ansari et al., 2025; Nalam et al., 2025), with the base chemical
196 mechanism (MOZART; Emmons et al., 2012) and source code modified to account for extra
197 tagged species representing regional and sectoral identities. Anthropogenic emissions of NO_x ,



198 CO, and non-methane volatile organic compounds (NMVOCs) are incorporated from the
199 Hemispheric Transport of Air Pollution version 3 emissions inventory. (HTAPv3; Crippa et
200 al., 2024), which includes land-based emissions, international shipping emissions, and aircraft
201 emissions. Biomass burning emissions are sourced from the GFED-v4 inventory (Van Der
202 Werf et al., 2010), while biogenic NMVOC emissions are derived from CAM4-GLOB-BIO-
203 v3.0. The O₃ source attribution technique used for this study is described in (Butler et al.,
204 2020).

205

206 **3. Results and discussions**

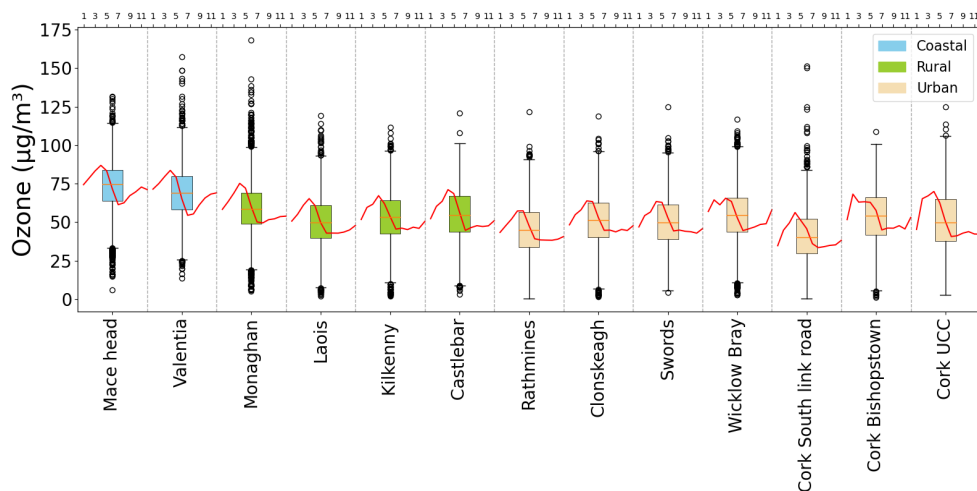
207 **3.1 Yearly variation of O₃**

208 Figure 2 shows box plots, illustrating the average O₃ concentrations for 13 sites over the
209 duration of the available dataset, as discussed in section 2.1 providing a comprehensive
210 overview of the variability and distribution of O₃ concentration. Coastal sites, such as Mace
211 Head, show higher O₃ levels compared to other sites, with an annual average concentration 77
212 µg/m³. Similarly, Valentia shows higher mean concentrations at 78 µg/m³ (in 2003). In urban
213 areas like Rathmines, Dublin, O₃ concentrations remained consistently lower, with averages
214 ranging from 39 to 56 µg/m³. Similarly, South link road and Bishopstown sites in Cork city,
215 recorded relatively lower concentrations compared to coastal and rural locations, reflecting the
216 impact of high urban NO_x emissions. Rural sites like Laois and Kilkenny showed intermediate
217 O₃ concentrations, less influenced by urban emissions. These sites consistently show O₃
218 averages ranging between 50 to 57 µg/m³, with little variability, highlighting the predominant
219 role of steady background O₃ contributions in rural sites. O₃ concentrations vary significantly
220 with proximity to emission sources – adjacent to urban areas, O₃ levels can be lower due to
221 titration, where O₃ reacts with NO, causing O₃ depletion, but the transport of precursors can



222 cause an increase in O_3 concentration downwind of the sources (Jeon et al., 2014; Monks et
223 al., 2015;Zhu et al., 2012)

224 The red line over the box shows a clear seasonal pattern in O_3 concentration for each site.
225 With a spring-time (March-April) peak and summer-time (June-July), dip, with the highest
226 peaks in the coastal sites, and lowest dips in urban sites, influenced by local emissions e.g.
227 Cork South Link Road and Swords.



228

229 **Figure 2.** Annual average O_3 concentration at different sites in Ireland. In each box, the lowest
230 whisker level represents the 5th percentile, the box spans from the 25th to the 75th percentile,
231 the horizontal line within the box represents the median 50th percentile, and the upper whisker
232 represents the 95th percentile. The average of monthly O_3 values calculated for the entire period
233 of each station, and the red line shows the average monthly O_3 variation of all sites top axis
234 shows the month (1– 12).

235 **3.2 O_3 Trend analysis**

236 **3.2.1 Yearly trend**



237 Table 2. summarizes the Theil-Sen trends in O₃ concentration (in µg/m³ per year) across 13
238 monitoring sites in Ireland over different periods: 5 years (2018-2022), 10 years (2013-2022),
239 15 years (2008-2022), and the available years of data for each site. In the coastal regions, Mace
240 Head shows a consistent decrease in O₃ levels over the 5, 10, and 15-year periods, although the
241 entire dataset exhibits a small rising trend 0.02 µg/m³ per year. These trends are mostly in
242 agreement with previous studies, where there was a positive trend observed in background O₃
243 up to the mid-2000s, which stabilised and began to decline in the 2010s (Derwent et al., 2018).
244 Valentia shows a long-term decreasing trend of -0.23 µg/m³ per year, consistent with the
245 previous study by Tripathi et al..2010.

246 In rural areas, Monaghan exhibits a declining trend in O₃ concentrations across all time periods,
247 indicating an overall reduction. Laois shows an upward trend over the 10 and 15-year periods,
248 though there is a slight decline in the most recent 5 years. Kilkenny presents slight negative
249 trends over the 5 and 10-year periods (-0.29 and -0.01µg/m³ per year). Negative trends are
250 observed in Castlebar-(0.71 and -0.05 µg/m³ per year).

251 The Dublin urban area sites (Rathmines, Clonskeagh, Swords) predominantly show increasing
252 trends in O₃ levels, indicative of changes in urban pollution or local emissions, with decreased
253 suppression of O₃ levels in urban regions due to decreased local emissions. (Derwent et al.,
254 2024). This is consistent with the “weekend effect,” as observed by (Atkinson-Palombo et al.,
255 2006)whereby a reduction in NO_x due to reduced weekend traffic decreases O₃ removal by
256 NO_x titration, leading to higher surface O₃ levels, likely to occur in wintertime, and in regions
257 with low photochemical production due to low insolation such as Ireland. Mixed results are
258 observed at the urban stations of Cork. This suggests variable factors affecting Cork O₃ levels.

259 Coastal sites like Mace Head and Valentia generally show decreasing trends, potentially due to
260 less local emission sources but with more significant impacts from regional and long-range



261 transport, However, a detailed analysis of the trends requires consideration of seasonal effects.

262 **Table 2.** - Trends in surface O₃ concentration (µg/m³ per year) calculated for 13 sites in Ireland

263 over different periods over the complete dataset: 5 years (2018-2022), 10 years (2013-2022),

264 15 years (2008-2022), and the available measurement record for the site. The p-value evaluates

265 the reliability of the trend, whereas a lower p-value indicates trend certainty. Adopting the trend

266 reliability scale defined for TOAR-II studies (Chang et al., 2023), trends with very high

267 certainty will be marked by ***($p \leq 0.001$), trends with high certainty with ** ($p \leq 0.01$), and

Site No	Site name (Classification)	Measurement Record	Trend over record µg/m ³ per year	5-year trend 2018-2022 µg/m ³ per year	10-year trend 2013-2022 µg/m ³ per year	15-year trend 2008-2022 µg/m ³ per year
1	Mace Head (C)	1994-2022	0.02	-0.25	-0.31*	-0.11
2	Valentia (C)	2001-2022	-0.23***	-1.15***	-0.84***	-0.32**
3	Monaghan (R)	1995-2022	-0.19***	-0.74**	-0.35*	-0.09*
4	Laois (R)	2005-2022	0.39***	-0.15	0.3**	0.46***
5	Kilkenny (R)	2012-2022	0.02	-0.29	-0.01	
6	Castlebar (R)	2009-2022	0.18*	-0.71*	-0.05	
7	Rathmines (U)	2002-2022	0.27***	1.72***	1.15***	0.48***
8	Clonskeagh (U)	2008-2022	0.33***	0.97**	0.12	0.33***
9	Swords (U)	2009-2022	0.6***	0.07	0.33***	
10	Wicklow Bray (U)	2009-2022	0.14*	0.04		
11	Cork South-link Road (U)	2014-2022	0.51*	-0.44		
12	Cork Bishopstown (U)	2016-2022	1.05**	-1.81*		
13	Cork UCC (U)	2018-2022	-0.94	-0.94		

268 low to medium certainty with *($p \leq 0.05$).

269 3.2.2 Monthly trend



Figure 3. shows the monthly trend for 10 years from the period 2012-2022. Mace Head (coastal) and Monaghan (rural) sites predominantly show a rising trend in winter/early spring, with a decreasing trend in late spring to summer. Valentia shows a decreasing trend in every month except February when levels are significantly impacted by long-range transport and stratospheric sources (Auvray and Bey, 2005; Pan et al., 2018). Urban sites show a general increasing trend, as yearly trend but with a seasonal signal in Clonskeagh an increase in winter-spring and a decrease in late spring or summer. Seasonal trends of the 15-year dataset are supplied in supplementary figure S2, where coastal stations exhibit a pronounced increase in early spring and a decrease in late summer, with a consistent near-year-round increase in urban stations of Rathmines and Laois.

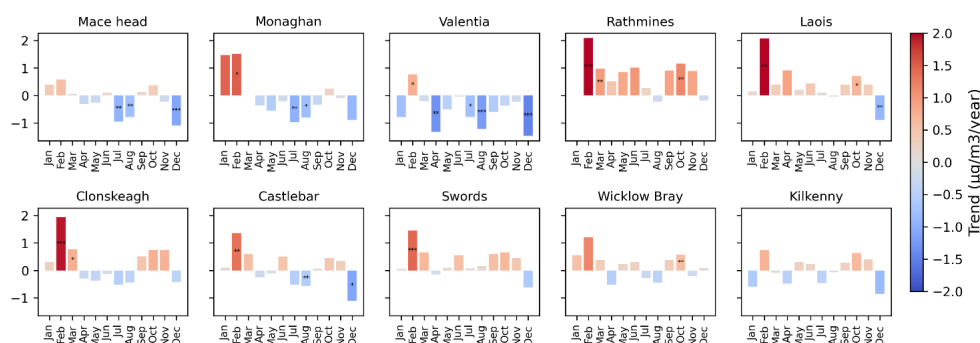


Figure 3. Monthly trend analysis of O_3 at different sites for 10 year period. (2012-2022) Adopting the trend reliability scale defined for TOAR-II studies (Chang et al., 2023), trends with very high certainty are marked by ***($p \leq 0.001$), trends with high certainty with **($p \leq 0.01$), and low to medium certainty with *($p \leq 0.05$). Positive trends are in red shade and negative trends are in blue shade.

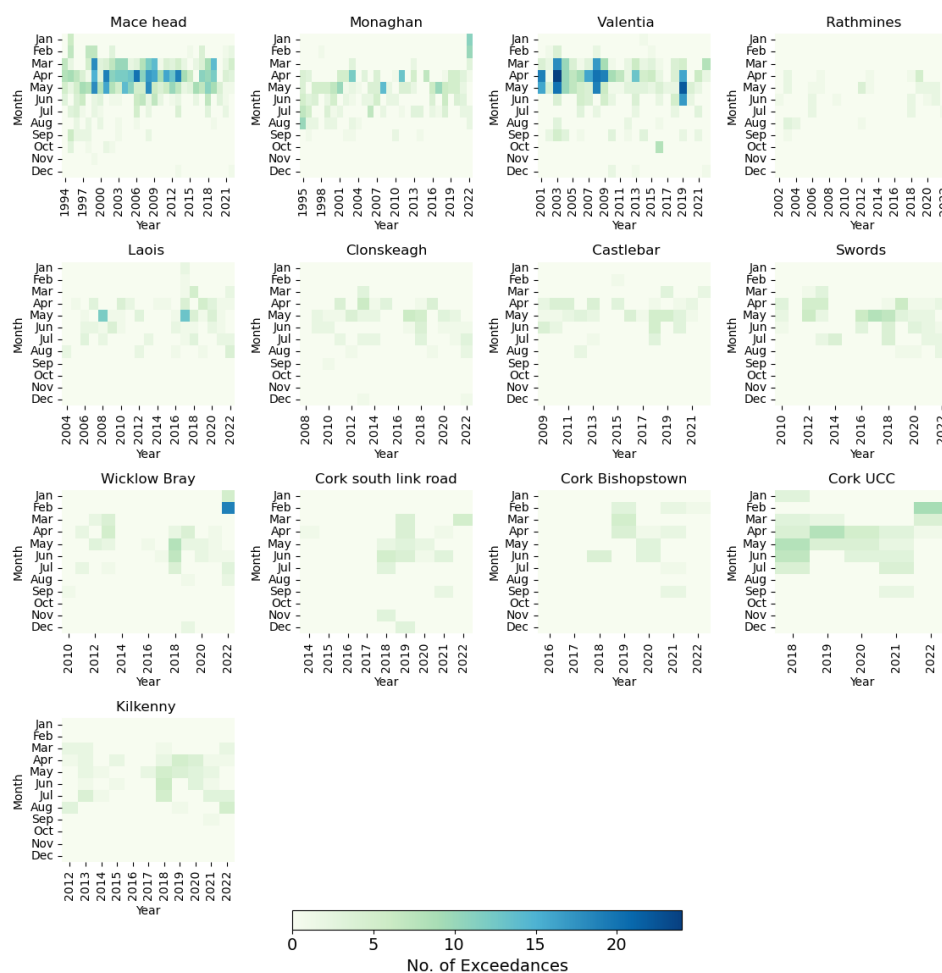


288 **3.3. O₃ Exceedance**

289 The O₃ exceedance are identified according WHO criteria and the results shown in figure 4.

290 It shows the monthly O₃ exceedances at 13 sites in Ireland over the available measurement
291 dataset. The highest and lowest numbers of O₃ exceedances were observed at Mace Head and
292 Rathmines, representing coastal and urban sites, respectively. Most exceedances occurred in
293 spring when O₃ concentrations were at a maximum.

294 Most sites recorded elevated spring-time occurrence in exceedances. E.g. Rathmines had its
295 highest number of exceedances in April 2019, while Laois reached a peak of 13 exceedances
296 in May 2017. Castlebar and Swords show increased exceedance occurrences in spring and
297 early summer, particularly notable spikes occurring in 2010, 2013, 2016, and 2019. Conversely,
298 Wicklow Bray exhibited a different pattern, showing significant spikes in February and March
299 2022, alongside occasional exceedances during March, April, and May, for example, in 2012
300 and 2018. Cork South link Road also recorded exceedances, particularly in March and June,
301 with significant spikes in 2018 and 2019. Cork Bishoptown shows exceedances, especially in
302 February and March 2019, while Cork UCC experienced spikes, particularly in April and May
303 2019. Kilkenny consistently exhibited exceedances during spring and summer, with April and
304 May often recording the highest number, particularly in 2019. This highlights the impact of
305 seasonal atmospheric conditions on O₃ levels. It is noted that summertime exceedances,
306 although less frequent in occurrence, indicate significant photochemical production that would
307 be required to elevate O₃ levels from the annual dip in the seasonal cycle to exceed the WHO
308 AQG threshold. These episodic spikes are characteristic of unique climatic or pollution events
309 and warrant further study.



310

311 **Figure 4.** - Monthly O₃ exceedance at different sites in Ireland.

312 Figure 5 depicts trends in NO₂ and CH₄ concentrations across various Irish measurement sites.

313 Most monitored sites exhibit a decreasing trend in NO₂ concentrations because of pollution

314 control on transportation, industrial activities, and energy production in the EU and North

315 America, in line with previous studies (Coleman et al., 2013; Donlon et al., 2024). In contrast,

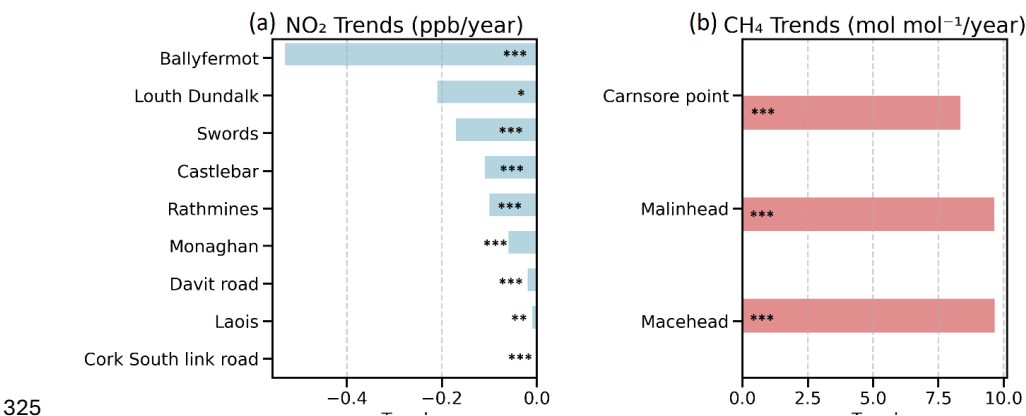
316 CH₄ levels at three sites Mace Head, Malin Head, and Carnsore Point indicate a significant and

317 persistent rise in CH₄ concentrations. Mace Head, known for its clean Atlantic air. Malin Head,

318 situated at Ireland's northern tip near the UK border, offers a unique position to observe both



319 clean marine air and transboundary pollution whereas Carnsore Point in the southeast, is
320 capture air masses from both the UK and mainland Europe, Carnsore Point receives the
321 majority of air masses from the land (Spohn et al., 2022). These NO₂ and CH₄ trends reveal a
322 dual dynamic: while NO₂ levels are decreasing due to effective emission controls, CH₄ levels
323 are rising unabated, highlighting the need for enhanced mitigation strategies targeting CH₄.
324

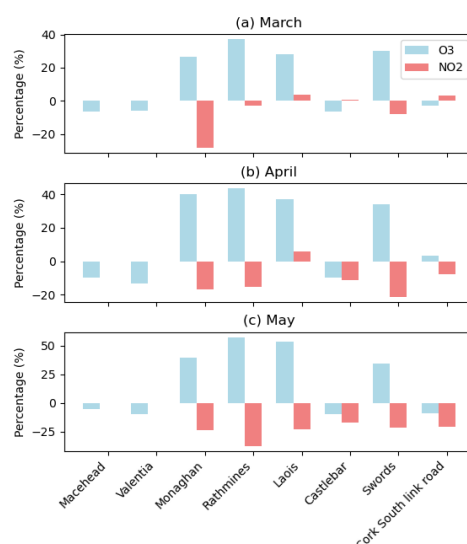


325
326 **Figure 5.-** Trend in O₃ precursors NO₂ (a), and CH₄ (b) at different sites. Trends with very high
327 certainty are marked by ***($p \leq 0.001$), trends with high certainty with **($p \leq 0.01$), and
328 low to medium certainty with *($p \leq 0.05$).

329 To evaluate the relationship between NO_x and O₃ concentrations in an Irish context and the
330 potential benefit of abrupt enforcement of NO_x control measures, we assess the impact of the
331 COVID-19 2020 lockdown, Spring 2020, whereby the lockdown period saw a prominent
332 relative decrease in NO₂, yet an increase in surface O₃ compared to average measurements for
333 the same months 2017-2019 in most national monitoring stations (Figure 6). The negative
334 correlation between O₃ and NO₂ is indicative of a NO_x-saturated regime, normally associated
335 with polluted urban environments and NO_x titration events. Similar results are discussed by
336 (Spohn et al., 2022) with meteorology. This effect was widely observed during the COVID



lockdown (Ordóñez et al., 2020; Tavella & da Silva Júnior, 2021; C. Zhang & Stevenson, 2022). Significant enhancement of O₃ occurs at the inland measurement sites, despite a 2020 spring-time decrease in O₃ observed at background coastal sites, Mace Head and Valentia. These coastal stations are less sensitive to changes in European NO_x emissions than inland sites and more sensitive to stratospheric and hemispheric transport (Tan et al., 2018). The atmospheric conditions in Ireland do not align with the interpretation of the atmosphere as being either a NO_x-controlled regime for clean environments or a NO_x-saturated regime in polluted environments. The negative correlation between NO_x and O₃, due to NO_x titration, observed in Ireland occurs under relatively clean atmospheric conditions, but it is consistent with low-insolation conditions, which are characteristic of Irish meteorology and frequent cloud cover ((Pall E E and Butler, n.d.)



348

349

350 **Figure 6.-** Percentage change in NO₂ and O₃ during the lockdown period of 2020 as compared
351 to the 2017-2019 average at different sites in Ireland for (a) March (b) April (c) May Month.

352 3.4 Model and Observations Comparison



3.4.1 Comparison between CAM4 – Chem Model and Observations

Global simulations were performed with the CAM4-Chem model enabled with source tagging (Butler et al., 2018) for 2000-2018 and the modelled O₃ over Ireland was compared with surface O₃ measurements at five sites. Figure 7 shows the comparison of monthly O₃ CAM4-Chem and ground station O₃ data. From this figure, it is observed that CAM4-Chem exhibits negative (positive) bias in rural and coastal (urban) sites. The underestimation at Mace Head is probably caused by the coarse grid resolution, covering a large area not representative of Mace Head conditions. The influence of coastal meteorology also leads to an underestimation of O₃ (Yerramilli et al 2012). Coastal meteorology, including cool sea surface temperatures and persistent clouds, suppresses O₃ formation. McVeigh et al., 2010 explained this through eddy correlation measurements showing downward ozone fluxes over coastal waters west of Ireland. The dry deposition rate over land would exceed that over the ocean leading to a lower simulated O₃ concentration for the entire grid cell. Dry deposition is enhanced by solar radiation (Coleman et al.,2012; Coleman et al., 2013; Pio et al., 2000) hence model measurement discrepancy is at a maximum in late summer months. Overestimation of O₃ in Clonskeagh and Cork South link Road is likely due to coarse grid handling of localised emissions and subsequent atmospheric chemistry.

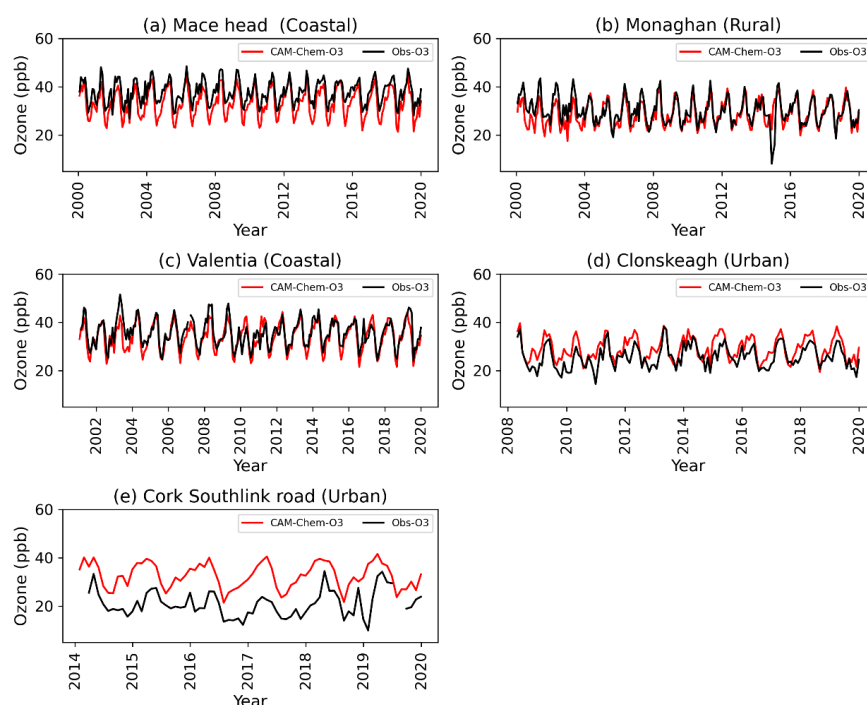


Figure 7. - The comparison of Monthly CAM4 – Chem O₃ and Monthly O₃ observations at five sites in Ireland.

At Mace Head, the model shows a negative mean bias of - 4.42 (-11.68% normalized mean bias) but strong correlation ($r=0.83$). In Monaghan and Valentia, the model shows smaller biases of -1.43 and -1.54, normalized mean biases of -4.74% and -1.54%, and correlation coefficients of 0.73 and 0.72, respectively. These high correlations are in line with (Tilmes et al., 2015). However, at Clonskeagh and Cork South Link Road, the model overestimates, with positive biases (3.38 and 11.98) and weaker correlations (0.68 and 0.49). Statistics are discussed in more detail in the supplementary material table S1. These results suggest better model performance at coastal/rural sites and greater discrepancies in urban areas as expected at this model resolution.

3.4.2 Source attribution using CAM4-Chem



384 To quantify the contribution of various precursor emission sources to modelled O₃
 385 concentrations, the TOAST1.0 dual NO_x and VOC tagging technique is utilised as described in
 386 (Butler et al., 2018). This allows us to attribute the modelled O₃ to the emissions of NO_x and
 387 VOC precursors across different source sectors and regions as listed in Table 3. The NO_x and
 388 VOC precursor emissions across different source sectors and regions, as shown in the Table,
 389 are responsible for the attribution of the modelled O₃.

390 **Table 3.** - List of tags used in NO_x and VOC tagging.

Regional Land-Based Tags		Regional Oceanic Tags		Global Sector/Process-Based Tags	
ARC	Arctic	NAL	North Atlantic	AIR	Aircraft
CAS	Central Asia	ENA	Eastern North Atlantic	BIO	Biogenic
EAS	East Asia	NAE	North America East Coast	BMB	Biomass Burning
EUR	Europe	NAW	North American West Coast	LGT	Lightning
MCA	Mexico & Central America	NPA	North Pacific	STR	Stratospheric Intrusion
MDE	Middle East	BNS	Baltic and North Seas	XTR	Extra untagged O ₃
NAF	North Africa	HBV	Hudson Bay	CH4	Methane
NAM	North America	IDO	Indian Ocean	OCN	Oceanic Sources (DMS)
RBU	Russia-Belarus-Ukraine	MBC	Mediterranean, Black, and Caspian Seas	SHP	Shipping
SAS	South Asia	SHO	Southern hemispheric oceans	AIR	Aircraft
SEA	Southeast Asia			INI	InitialConditionO ₃
VRW	Rest of the World				

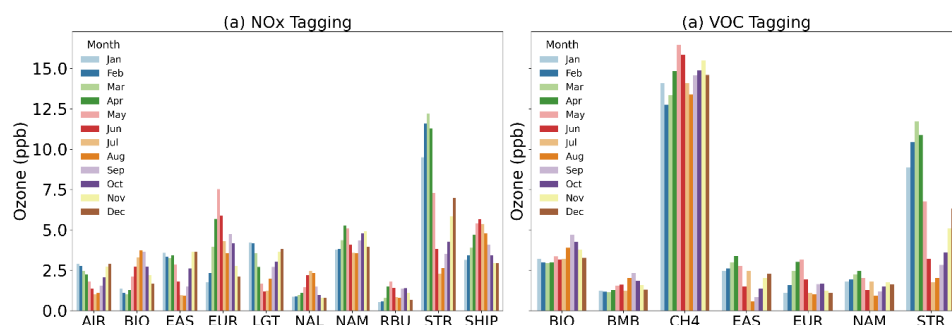
391



392 The monthly tagged major precursor contributions to surface O_3 at Mace Head, averaged over
393 the 2000-2018 simulation period, are shown in Figure 8. The stratospheric source of O_3
394 dominates in Winter-Spring, contributing to the spring-time maxima due to vigorous
395 stratospheric transport. European NO_x emissions contribution peaks in May, while lightning
396 NO_x has the greatest impact in winter. North American emissions contribute 3.5 to 5.25 ppb,
397 peaking in April, and aviation emissions contribute 1 to 3 ppb, with the highest contributions
398 in winter and spring. Biogenic NO_x , significant between June and October, contributes an
399 average of 3.6 ppb, with higher contributions during August and September. Biogenic VOC
400 sources contribute slightly more, averaging over 4 ppb during late autumn and maintaining a
401 more sustained contribution throughout the year. East Asian NO_x emissions, contributing up to
402 3.6 ppb, show a minimum contribution in July and August. North Atlantic shipping NO_x (NAL)
403 accounts for up to 2.4 ppb of O_3 during July month. The total shipping NO_x (SHIP) also
404 contributes significantly and shows the highest contribution in June month.

405 Methane (CH_4) is the dominant reactive carbon molecule contributing to O_3 formation. VOC
406 emissions from biomass burning also play a measurable role, contributing 1 to 2 ppb, with their
407 largest contributions in August and September. Finally, European VOC emissions contribute 1
408 to 3 ppb, with the largest impact from March to May, coinciding with the spring-time peak in
409 surface O_3 . These findings allow quantification of specific sources amidst the complex
410 interplay of regional and global sources in driving seasonal variations in surface O_3 levels over
411 the Irish domain, highlighting the roles of stratospheric processes, anthropogenic emissions,
412 biogenic sources, and lower-latitude contributions in shaping the observed patterns at
413 background monitoring sites such as Mace Head.

414



415

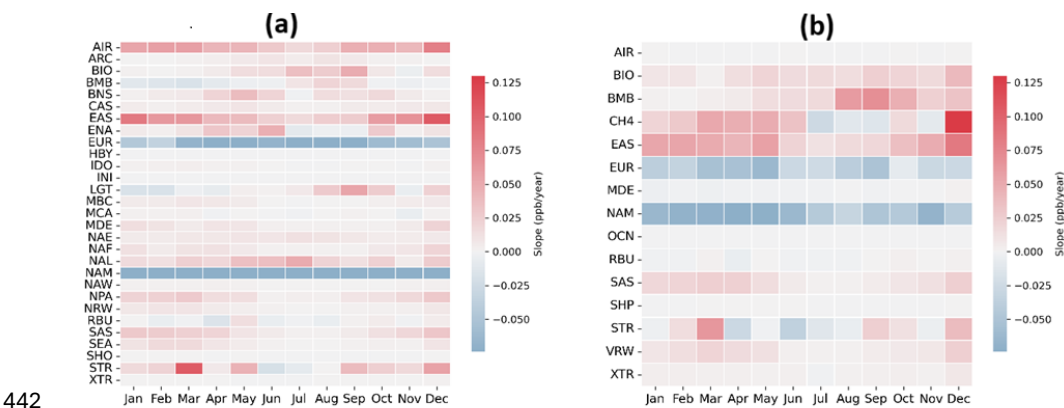
416 **Figure 8.-** Absolute contribution of major NO_x sources (a) (NO_x Tagging) and VOC source
417 (b) (NO_x Tagging) to the CAM4-Chem simulated surface O₃ for the Mace Head grid cell
418 between 2000-2018.

419 Figure 9 shows the monthly changes in contributions to surface O₃ at Mace Head over the
420 simulation period (2000-2018). A negative (blue) trend indicates that the contribution of the
421 source to simulated surface O₃ in this grid cell has declined over the simulation period, whereas
422 a positive trend (red) indicates the contribution to surface O₃ has risen. Figure 9 (a) indicates
423 that the amount of simulated O₃ at Mace Head originating from European or North American
424 NO_x decreases during the simulation period, consistent with EU & North American emission
425 reductions over the period (, (Guerreiro et al., 2014;US EPA 2027), with more significant
426 reduction occurring in late Spring through late summer, when EU NO_x contributions are most
427 significant to Mace Head O₃ concentrations (as seen in Figure 8).

428 There is a rising trend in simulated surface O₃ originating from NO_x emissions from global
429 aviation, from East Asia, and to a lesser extent from South Asia, which is more pronounced in
430 the wintertime. This seasonality in source contributions explains the observed reduction in
431 spring-time maxima and increase in winter-time levels from the measurement record. East-
432 Asian and South-Asian VOCs also contribute to a rising trend in simulated O₃, with a more
433 pronounced increase in winter and spring. This highlights a different pattern in hemispheric O₃
434 contributions, where emission reductions in Europe and North America are accompanied by



435 increased influence from lower latitudes. This increasing contribution could become a more
436 important source of background O₃ in the future. The contribution of CH₄ also has a positive
437 trend over the simulation period, but the CH₄ trend has a reliable correlation only in the
438 December and spring periods, with no observed trend during the summer months when
439 atmospheric CH₄ trends have very low certainty (correlation coefficient, $p > 0.33$) consistent
440 with decline in local NO_x emissions in Europe. The Anthropogenic VOC contributions from
441 Europe (EUR) and North America (NAM) show a negative trend for all months.



442
443 **Figure 9.** Trends in contributions to monthly average modelled Mace Head grid cell surface
444 O₃ at for the 2000-2018 period derived from (a) NO_x tagging and (b) VOC tagging.

445 Table 4. shows the overall trend in the main contributors to NO_x and VOC tagging. It is
446 observed that there is an increase in simulated surface O₃ originating from NO_x contributions,
447 from aviation and East Asia, while there is a decrease in European (EUR) and North American
448 (NAM) NO_x contributions. In VOC tagging, Methane (CH₄) and East Asian anthropogenic
449 VOC (EAS) contribute to a rising trend over the simulation period, whereas anthropogenic
450 VOC contributions from Europe (EUR) and North America (NAM) show a negative trend.

451 **Table 4 - Overall Trend in contributions to Mace Head grid cell O₃ simulated by CAM4-Chem**
452 for NO_x tagging and VOC tagging over the simulation period in units of ppb per year. The



453 trend with very high certainty is marked by $*** (p \leq 0.001)$, trends with high certainty with
454 $** (p \leq 0.01)$, and low to medium certainty with $* (p \leq 0.05)$.

NO _x Tagging		VOC Tagging	
	Slope (ppb/year)		Slope (ppb/year)
AIR	0.0467***	CH ₄	0.0590***
EAS	0.0491***	EAS	0.0333***
EUR	-0.0900***	EUR	-0.0553***
NAM	-0.1243***	NAM	-0.0670***

455

456 3.5 O₃ Trends in Background and EU influenced sector Air masses at Mace Head

457 Although Mace Head is classified as a global background site, quantification of the baseline
458 pollution levels requires filtering the data to limit the data to that arriving from the clean sector.
459 Based on the trajectories filtering of Mace head O₃ measurement data discussed in section 2.5.
460 From figure 10 O₃ observations shows clean sector consistently has higher O₃ concentrations
461 than the EU influenced sector especially during the annual spring-time high, indicating a longer
462 lifetime for O₃ over the North Atlantic, and the land mass and pollution sources are acting as a
463 sink for O₃ in the Irish context (Fowler et., al 2008). A decreasing trend in spring-time levels
464 is observed for both clean and EU influenced sectors, consistent with the decrease in precursor
465 emissions in Europe and North America. There is a significant difference between clean, and
466 EU influenced sector measurements, the influence of EU influenced sector air to scavenge O₃
467 via NO_x titration, leading to higher O₃ in clean-sector air masses, as also found in previous
468 studies (Coleman et al., 2013). An increasing trend is observed in the winter-time EU influenced
469 sector, which is not observed in the clean sector. This would infer a decrease in winter-time O₃
470 depletion events due to decreasing European emissions (from the EU influenced sector),
471 consistent with the conclusions from previous studies of Mace Head surface O₃ (Derwent et
472 al., 2024). Summer-time values do not exhibit a notable trend or a discrepancy between clean



473 and EU influenced sector measurements, indicating that there is little O₃ advected into Europe
474 from the west in the summer months. Autumn values show higher O₃ in the clean sector, but
475 without a significant slope.

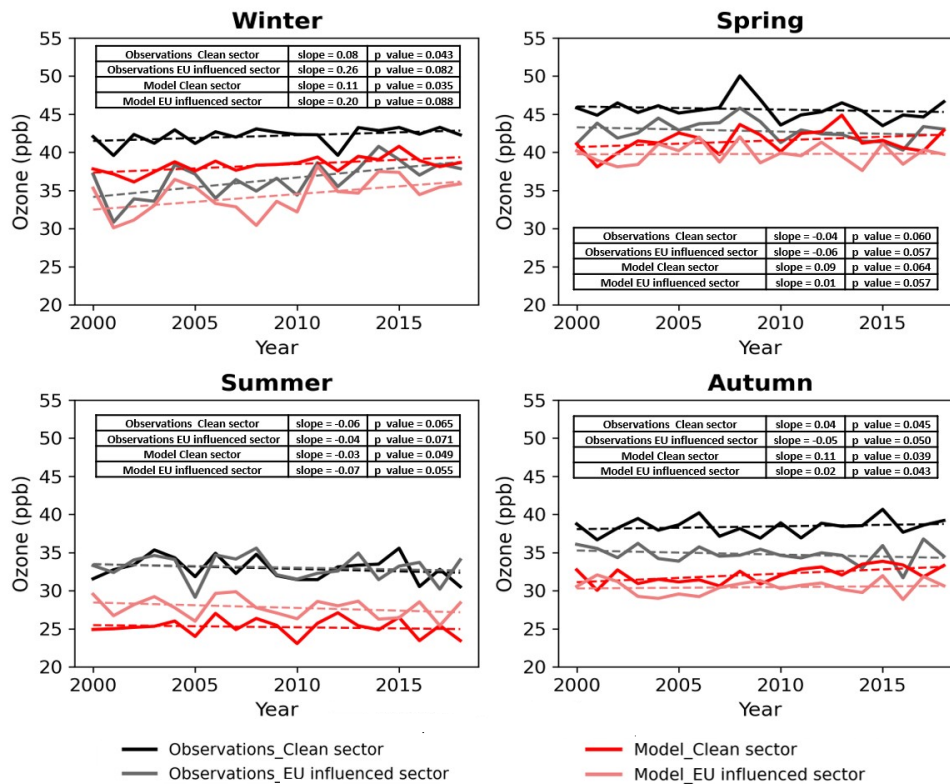
476 The model results indicate that the clean sector consistently exhibits higher O₃ concentrations
477 than the EU-influenced sector, except during the summer season. In the winter season, a
478 significant increasing trend is observed for both sectors, which aligns well with the O₃
479 observations. A decreasing trend is observed during the summer season, consistent with the
480 observations for both sectors. In spring and autumn, a positive trend is observed.

481 Trends in contributors of model O₃ during the different seasons for the clean and EU-
482 influenced sector are shown in Tables S3 to S4 in the supplementary material. Aviation and
483 East Asian NO_x shows consistently positive and significant trends in both sectors, while North
484 America NO_x shows strong negative trends throughout the year in the clean sector. For the
485 EU-influenced sector in NO_x tagged (Table S2), similar positive trends observed for aviation
486 and East Asian, with North America NO_x remaining negative and European NO_x showing more
487 significant declines in spring and winter. In case of VOC tagged O₃, the East Asian VOCs
488 shows an increasing trend and North America VOCs negative across all seasons in both sectors
489 (Table S3 and S4). European VOCs also show a consistent negative trend, particularly strong
490 in the EU-influenced sector. Methane trends are seasonally positive, especially in spring and
491 winter.

492 It is observed that the model consistently simulates O₃ at lower concentrations than that
493 observed at Mace Head. This is not surprising, considering the coarse resolution of the model,
494 which limits its ability to represent fine-scale processes and dry deposition accurately. Dry
495 deposition is typically higher over land, and the grid cell covering Mace Head includes land
496 area, as shown in Figure S5 of the supplementary material. Further, as explained by Fiore et al.



497 (2009), models average the landscape characteristics within a grid cell, which can enhance O₃
498 deposition and result in lower simulated O₃ concentrations; hence, the discrepancy is more
499 pronounced in the clean sector data.



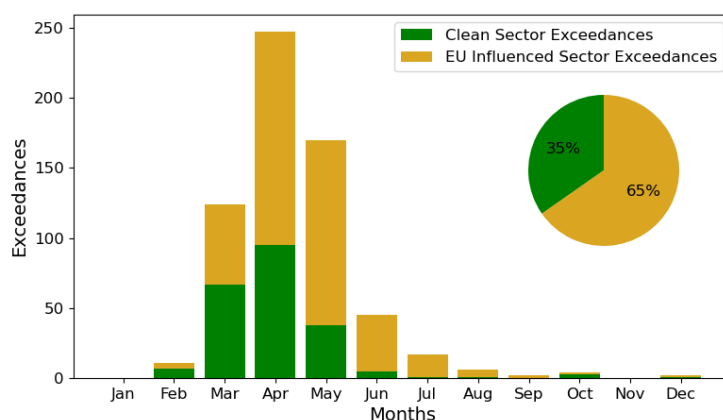
500
501 **Figure 10.** - Trend in seasonal Average of observed O₃ (black) and Model O₃ (red) at Mace
502 head, separated into clean sector and EU-influenced sector.

503 3.6 Exceedances from the clean and EU-influenced sector at Mace Head

504 Exceedances observed at Mace Head between 2000 and 2022 are separated into clean and EU-
505 influenced sectors based on trajectory air masses and shown in Figure 11. 33% of all
506 exceedances for this period occurred in clean air masses, the remainder occurring when O₃-EU



507 influenced sector air is advected over Ireland and local land masses to enhance surface O_3 ,
508 which is already elevated at Mace Head compared to inland and urban sites.



509

510 **Figure 11.** - Exceedances measured at Mace Head per month from 2000 until 2022, during the
511 clean air sector (green) and EU influenced sector (yellow). The percentage of both to total
512 exceedances is shown in the inset.

513 Figure 12 shows the trend in spring-time exceedances and the 95th percentile Spring-time O_3
514 measured at Mace Head between 2000 and 2022. A decreasing trend in exceedances and clean
515 sector spring-time exceedances is observed, with a greater decreasing trend in the total number
516 of exceedances. This indicates that the changes that are driving the reduction in the exceedances
517 in Europe are coming into effect at a quicker rate than the changes that are driving O_3 event
518 reduction over the North Atlantic. The trends in the exceedance counts are not significant,
519 according to the criteria in Chang et al., 2023, but there is a statistically significant decreasing
520 trend in the 95th percentile springtime surface O_3 over the measurement record. Figure 12 (b)
521 shows the trend in spring-time surface O_3 measured at Mace Head segregated into Clean and
522 EU-influenced sector. The trend is more significant both in magnitude and statistical certainty
523 for the EU-influenced sector, indicating EU emission changes having a more pronounced effect



on spring-time O₃ measured at Mace Head O₃ as compared to changes affecting O₃ transported
or formed over the North Atlantic.

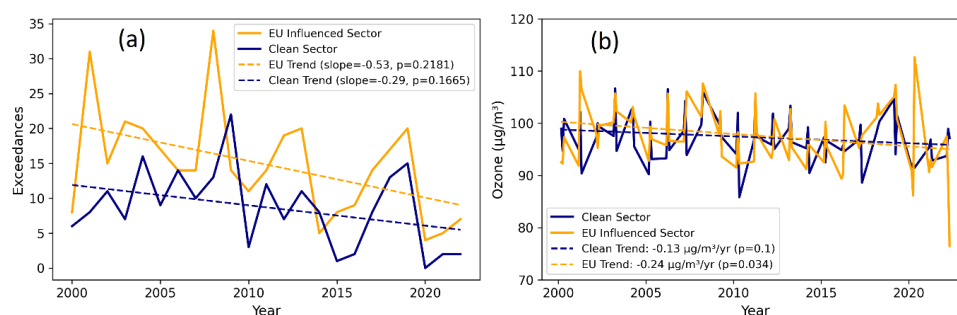
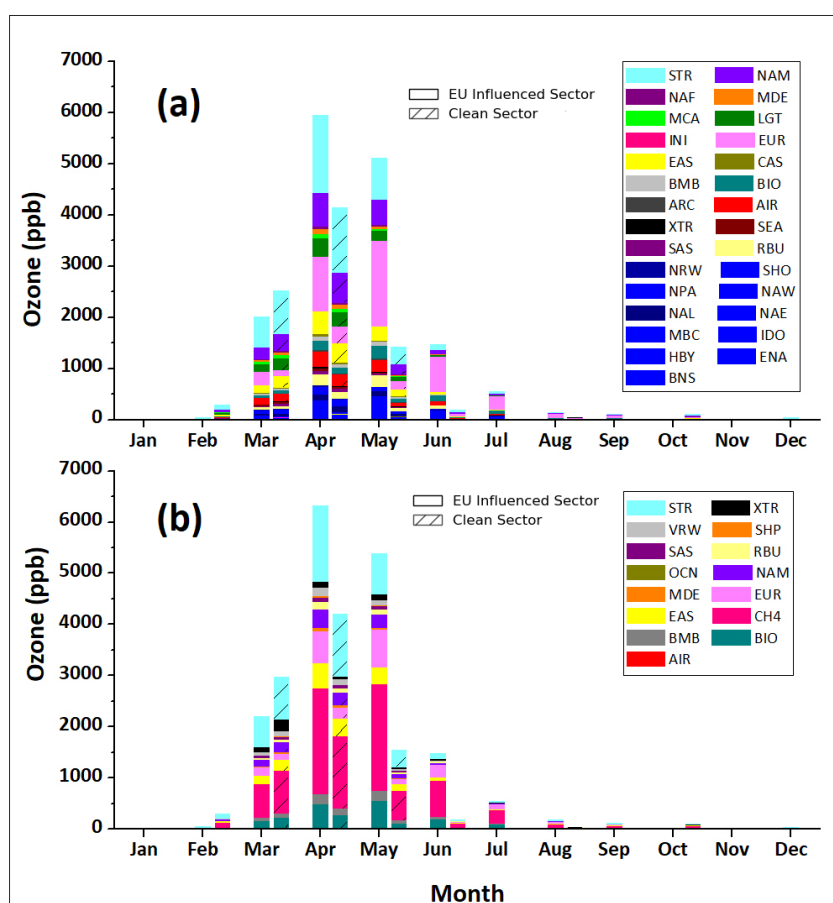


Figure 12. (a) The trend in Spring-time exceedances measured at Mace Head between 2000 and 2022 (blue) with the clean-air exceedances (gold), and (b) The trend in 95th percentile of spring (Mar- May) O₃ measured in µg /m³ for the clean sector (blue) and the EU-influenced sector (gold).

Figure 13 shows monthly cumulative contributions to simulated O₃ concentrations within the Mace Head grid cell for NO_x and VOC tagging during O₃ exceedance, which is observed from O₃ observations calculated as discussed in section 3.3. In addition, these exceedances are categorised into clean and EU-influenced sectors. The maximum exceedances are observed in March to May month. From Figure 13 (a), it is clear that stratospheric intrusion, North American NO_x, European NO_x, and East Asian NO_x are the major contributors driving exceedances at Mace Head during the spring months (March to May). Among these, European emissions dominate the supply of NO_x precursors in April, reaching their peak in May. Figure 13 (b) shows that CH₄ is the most dominant source, followed by stratospheric intrusion and Biomass burning. North American and European VOC emissions also contribute significantly to O₃ formation during this period. Collectively, these findings highlight the complex interplay of regional and global sources in driving surface O₃ exceedances over the Irish domain.



543 The cumulative O₃ contributions to EU-influenced sector and clean sector exceedances for
544 NO_x tagging and VOC tagging, it is clear that the North American NO_x also contributes
545 significantly to exceedance in both clean and EU-influenced sectors at Mace Head during
546 March to May months. It may be due to transport and mixing, regional stagnation or synoptic-
547 scale recirculation. In the case of VOC tagging, stratospheric intrusion, and CH₄ show notable
548 contributions. Biomass burning, East Asian emissions and North American VOC emissions
549 also play a role in O₃ exceedances.



550



551 **Figure 13** - Monthly cumulative Mace Head grid cell O_3 contributions to EU influenced
552 sector and clean sector exceedances (a) NO_x tagging and (b) VOC tagging Mace Head grid
553 cell.

554

555 **4. Conclusion**

556 This study highlights the complexities of O_3 pollution in Ireland, revealing that coastal areas
557 experience higher O_3 concentrations than rural and urban environments, attributed to the effect
558 of transboundary pollution and stratospheric intrusion. Over the last two decades, urban sites
559 have shown a significant increasing trend in O_3 levels, likely influenced by decreasing nitrogen
560 oxides (NO_x) in Europe, including Ireland, and North America. The analysis also points out
561 that exceedances at coastal monitoring sites correlate with years of higher spring maxima,
562 driven mainly by hemispheric transport and stratospheric influences(16%). Utilising the
563 advanced capabilities of the CAM4-Chem model with dual NO_x and VOC tagging, we
564 identified key factors affecting seasonal O_3 variations, such as the spring-time peak and
565 summer dip, driven by a mix of stratospheric intrusion, hemispheric transport, and regional
566 emissions. Trend analysis from simulation results identified East Asian and aviation emissions
567 as significant contributors to the rising winter trends in O_3 , while reductions in North American
568 and European emissions accounted for the decrease in spring peaks. This study provides a
569 comprehensive understanding of the various factors affecting O_3 levels in Ireland, offering
570 important insights for the development of O_3 pollution control policies.

571

572 **Data availability**

573 All data are available upon request.



574 **Author contributions**

575 LC designed the study. NK analyzed the data and wrote the manuscript. TA and TB provided
576 CAM-Chem model results and reviewed the manuscript.. JO and CD reviewed the manuscript
577 and edited it.LC edited it with contributions from all coauthors

578 **Competing interests**

579 The authors declare that at least one of the authors sits on the editorial board of ACP.

580 **Acknowledgement** - The authors acknowledge the Environmental Protection Agency (EPA)
581 of Ireland for their financial support of the Ozone project under the EPA Research Programme
582 2021-2030 (project number 2022-CE-1133), and the European Union's Horizon Europe
583 Research and Innovation programme under HORIZON-CL5-2022-D1-02 (grant no.
584 101081430-PARIS).

585

586 **References**

587 Aghedo, A. M., Bowman, K. W., Worden, H. M., Kulawik, S. S., Shindell, D. T., Lamarque, J.
588 F., Faluvegi, G., Parrington, M., Jones, D. B. A., and Rast, S.: The vertical distribution of ozone
589 instantaneous radiative forcing from satellite and chemistry climate models, Journal of
590 Geophysical Research Atmospheres, 116, <https://doi.org/10.1029/2010JD014243>, 2011.

591 Anenberg, S. C., West, J. J., Fiore, A. M., Jaffe, D. A., Prather, M. J., Bergmann, D., Cuvelier,
592 K., Dentener, F. J., Duncan, B. N., Gauss, M., Hess, P., Jonson, J. E., Lupu, A., Mackenzie, I.
593 A., Marmer, E., Park, R. J., Sanderson, M. G., Schultz, M., Shindell, D. T., Szopa, S., Vivanco,
594 M. G., Wild, O., and Zeng, G.: Intercontinental impacts of ozone pollution on human mortality,
595 Environ Sci Technol, 43, 6482–6487, <https://doi.org/10.1021/es900518z>, 2009.



- 596 Ansari, T., Nalam, A., Lupaşcu, A., Hinz, C., Grasse, S., and Butler, T.: Explaining trends and
597 changing seasonal cycles of surface ozone in North America and Europe over the 2000–2018
598 period: A global modelling study with NO_x and VOC tagging,
599 <https://doi.org/10.5194/egusphere-2024-3752>, 13 December 2024.
- 600 Archibald, A. T., Neu, J. L., Elshorbany, Y. F., Cooper, O. R., Young, P. J., Frost, G. J., Galbally,
601 I. E., Gerosa, G., Granier, C., and Griffiths, P. T.: Tropospheric Ozone Assessment Report : A
602 critical review of changes in the tropospheric ozone burden and budget from 1850 to 2100, 1–
603 53, 2020.
- 604 Ashmore, M. R.: Assessing the future global impacts of ozone on vegetation, *Plant Cell*
605 *Environ*, 28, 949–964, <https://doi.org/10.1111/j.1365-3040.2005.01341.x>, 2005.
- 606 Atkinson-Palombo, C. M., Miller, J. A., and Balling, R. C.: Quantifying the ozone “weekend
607 effect” at various locations in Phoenix, Arizona, *Atmos Environ*, 40, 7644–7658,
608 <https://doi.org/10.1016/j.atmosenv.2006.05.023>, 2006.
- 609 Auvray, M. and Bey, I.: Long-range transport to Europe: Seasonal variations and implications
610 for the European ozone budget, <https://doi.org/10.1029/2004JD005503>, 16 June 2005.
- 611 Bessagnet, B., Pirovano, G., Mircea, M., Cuvelier, C., Aulinger, A., Calori, G., Ciarelli, G.,
612 Manders, A., Stern, R., Tsyro, S., García Vivanco, M., Thunis, P., Pay, M. T., Colette, A.,
613 Couvidat, F., Meleux, F., Rouil, L., Ung, A., Aksoyoglu, S., Baldasano, J. M., Bieser, J.,
614 Briganti, G., Cappelletti, A., D’Isidoro, M., Finardi, S., Kranenburg, R., Silibello, C.,
615 Carnevale, C., Aas, W., Dupont, J. C., Fagerli, H., Gonzalez, L., Menut, L., Prévôt, A. S. H.,
616 Roberts, P., and White, L.: Presentation of the EURODELTA III intercomparison exercise-
617 evaluation of the chemistry transport models’ performance on criteria pollutants and joint
618 analysis with meteorology, *Atmos Chem Phys*, 16, 12667–12701, [https://doi.org/10.5194/acp-](https://doi.org/10.5194/acp-16-12667-2016)
619 16-12667-2016, 2016.



- 620 Boylan, P., Helmig, D., and Oltmans, S.: Ozone in the Atlantic Ocean marine boundary layer,
621 1–13, <https://doi.org/10.12952/journal.elementa.000045>, 2014.
- 622 Butchart, N., Charlton-Perez, A. J., Cionni, I., Hardiman, S. C., Haynes, P. H., Krüger, K.,
623 Kushner, P. J., Newman, P. A., Osprey, S. M., Perlwitz, J., Sigmond, M., Wang, L., Akiyoshi,
624 H., Austin, J., Bekki, S., Baumgaertner, A., Braesicke, P., Brhl, C., Chipperfield, M., Dameris,
625 M., Dhomse, S., Eyring, V., Garcia, R., Garny, H., Jöckel, P., Lamarque, J. F., Marchand, M.,
626 Michou, M., Morgenstern, O., Nakamura, T., Pawson, S., Plummer, D., Pyle, J., Rozanov, E.,
627 Scinocca, J., Shepherd, T. G., Shibata, K., Smale, D., Teyssède, H., Tian, W., Waugh, D., and
628 Yamashita, Y.: Multimodel climate and variability of the stratosphere, *Journal of Geophysical*
629 *Research Atmospheres*, 116, <https://doi.org/10.1029/2010JD014995>, 2011.
- 630 Butler, T., Lupascu, A., Coates, J., and Zhu, S.: TOAST 1.0: Tropospheric ozone attribution of
631 sources with tagging for CESM 1.2.2, *Geosci Model Dev*, 11, 2825–2840,
632 <https://doi.org/10.5194/gmd-11-2825-2018>, 2018.
- 633 Butler, T., Lupascu, A., and Nalam, A.: Attribution of ground-level ozone to anthropogenic and
634 natural sources of nitrogen oxides and reactive carbon in a global chemical transport model,
635 *Atmos Chem Phys*, 20, 10707–10731, <https://doi.org/10.5194/acp-20-10707-2020>, 2020.
- 636 Carslaw, D. C.: On the changing seasonal cycles and trends of ozone at Mace Head, Ireland,
637 *Atmos. Chem. Phys*, 3441–3450 pp., 2005.
- 638 Chang, K.-L., Schultz, M. G., Koren, G., and Selke, N.: Guidance note on best statistical
639 practices for TOAR analyses, 2023.
- 640 Coleman, L., McVeigh, P., Berresheim, H., Martino, M., and O’Dowd, C. D.: Photochemical
641 impact on ozone fluxes in coastal waters, *Advances in Meteorology*, 2012,
642 <https://doi.org/10.1155/2012/943785>, 2012.



- 643 Coleman, L., Martin, D., Varghese, S., Jennings, S. G., and O'Dowd, C. D.: Assessment of
644 changing meteorology and emissions on air quality using a regional climate model: Impact on
645 ozone, *Atmos Environ*, 69, 198–210, <https://doi.org/10.1016/j.atmosenv.2012.11.048>, 2013.
- 646 Creilson, J. K., Fishman, J., & Wozniak, A. E. Intercontinental transport of tropospheric ozone:
647 A study of its seasonal variability across the North Atlantic utilizing tropospheric ozone
648 residuals and its relationship to the North Atlantic Oscillation. *Atmospheric Chemistry and*
649 *Physics*, 3(6), 2053–2066. <https://doi.org/10.5194/acp-3-2053-2003>, 2003.
- 650 Crippa, M., Guizzardi, D., Pagani, F., Schiavina, M., Melchiorri, M., Pisoni, E., Graziosi, F.,
651 Muntean, M., Maes, J., Dijkstra, L., Van Damme, M., Clarisse, L., and Coheur, P.: Insights into
652 the spatial distribution of global, national, and subnational greenhouse gas emissions in the
653 Emissions Database for Global Atmospheric Research (EDGAR v8.0), *Earth Syst Sci Data*, 16,
654 2811–2830, <https://doi.org/10.5194/essd-16-2811-2024>, 2024.
- 655 Derwent, R. G.: OBSERVATION AND INTERPRETATION OF THE SEASONAL CYCLES
656 IN THE SURFACE CONCENTRATIONS OF OZONE AND CARBON MONOXIDE AT
657 MACE HEAD , IRELAND FROM 1990 TO 1994, 2310, 1998.
- 658 Derwent, R. G., Simmonds, P. G., and Collins, W. J.: Ozone and carbon monoxide
659 measurements at a remote maritime location, mace head, Ireland, from 1990 to 1992, *Atmos*
660 *Environ*, 28, 2623–2637, [https://doi.org/10.1016/1352-2310\(94\)90436-7](https://doi.org/10.1016/1352-2310(94)90436-7), 1994.
- 661 Derwent, R. G., Jenkin, M. E., Saunders, S. M., and Pilling, M. J.: Photochemical ozone
662 creation potentials for organic compounds in northwest Europe calculated with a master
663 chemical mechanism, *Atmos Environ*, 32, 2429–2441, [https://doi.org/10.1016/S1352-](https://doi.org/10.1016/S1352-2310(98)00053-3)
664 [2310\(98\)00053-3](https://doi.org/10.1016/S1352-2310(98)00053-3), 1998.
- 665 Derwent, R. G., Collins, W. J., Johnson, C. E., and Stevenson, D. S.: Transient behaviour of
666 tropospheric ozone precursors in a global 3-d ctm and their indirect greenhouse effects, 2001.



- 667 Derwent, R. G., Stevenson, D. S., Collins, W. J., and Johnson, C. E.: Intercontinental transport
668 and the origins of the ozone observed at surface sites in Europe, *Atmos Environ*, 38, 1891–
669 1901, <https://doi.org/10.1016/j.atmosenv.2004.01.008>, 2004.
- 670 Derwent, R. G., Stevenson, D. S., Doherty, R. M., Collins, W. J., and Sanderson, M. G.: How
671 is surface ozone in Europe linked to Asian and North American NO_x emissions?, *Atmos*
672 *Environ*, 42, 7412–7422, <https://doi.org/10.1016/j.atmosenv.2008.06.037>, 2008.
- 673 Derwent, R. G., Manning, A. J., Simmonds, P. G., Spain, T. G., and O’Doherty, S.: Analysis
674 and interpretation of 25 years of ozone observations at the Mace Head Atmospheric Research
675 Station on the Atlantic Ocean coast of Ireland from 1987 to 2012, *Atmos Environ*, 80, 361–
676 368, <https://doi.org/10.1016/j.atmosenv.2013.08.003>, 2013.
- 677 Derwent, R. G., Manning, A. J., Simmonds, P. G., and Doherty, S. O.: Long-term trends in
678 ozone in baseline and European regionally-polluted air at Mace Head , Ireland over a 30-year
679 period, *Atmos Environ*, 179, 279–287, <https://doi.org/10.1016/j.atmosenv.2018.02.024>, 2018a.
- 680 Derwent, R. G., Manning, A. J., Simmonds, P. G., Spain, T. G., and O’Doherty, S.: Long-term
681 trends in ozone in baseline and European regionally-polluted air at Mace Head, Ireland over a
682 30-year period, *Atmos Environ*, 179, 279–287,
683 <https://doi.org/10.1016/j.atmosenv.2018.02.024>, 2018b.
- 684 Derwent, R. G., Parrish, D. D., Manning, A. J., Spain, T. G., Simmonds, P. G., and O’Doherty,
685 S.: Ozone at Mace Head, Ireland from 1987 to 2021: Declining baselines, phase-out of
686 European regional pollution, COVID-19 impacts, *Atmos Environ*, 320,
687 <https://doi.org/10.1016/j.atmosenv.2023.120322>, 2024.
- 688 Ding, J., Dai, Q., Fan, W., Lu, M., Zhang, Y., Han, S., and Feng, Y.: Impacts of meteorology
689 and precursor emission change on O₃ variation in Tianjin, China from 2015 to 2021, *J Environ*
690 *Sci (China)*, 126, 506–516, <https://doi.org/10.1016/j.jes.2022.03.010>, 2023.



- 691 Donlon, B., Cahalane, A., and Fanning, A.: Ireland's State of the Environment Report 2024
692 Editors, 2024.
- 693 Draxler, R. R. Evaluation of an Ensemble Dispersion Calculation.
694 <http://wesley.wwb.noaa.gov/reanalysis.html>, 2003.
- 695 EEA. Trends and projections in Europe 2024. <https://doi.org/10.2800/7574066>, 2024.
- 696 Fiore, A. M., Dentener, F. J., Wild, O., Cuvelier, C., Schultz, M. G., Hess, P., Textor, C., Schulz,
697 M., Doherty, R. M., Horowitz, L. W., MacKenzie, I. A., Sanderson, M. G., Shindell, D. T.,
698 Stevenson, D. S., Szopa, S., Van Dingenen, R., Zeng, G., Atherton, C., Bergmann, D., Bey, I.,
699 Carmichael, G., Collins, W. J., Duncan, B. N., Faluvegi, G., Folberth, G., Gauss, M., Gong, S.,
700 Hauglustaine, D., Holloway, T., Isaksen, I. S. A., Jacob, D. J., Jonson, J. E., Kaminski, J. W.,
701 Keating, T. J., Lupu, A., Manner, E., Montanaro, V., Park, R. J., Pitari, G., Pringle, K. J., Pyle,
702 J. A., Schroeder, S., Vivanco, M. G., Wind, P., Wojcik, G., Wu, S., and Zuber, A.: Multimodel
703 estimates of intercontinental source-receptor relationships for ozone pollution, *Journal of*
704 *Geophysical Research Atmospheres*, 114, <https://doi.org/10.1029/2008JD010816>, 2009.
- 705 Fowler, D., Coyle, M., Skiba, U., Sutton, M. A., Cape, J. N., Reis, S., Sheppard, L. J., Jenkins,
706 A., Grizzetti, B., Galloway, J. N., Vitousek, P., Leach, A., Bouwman, A. F., Butterbach-Bahl,
707 K., Dentener, F., Stevenson, D., Amann, M., and Voss, M.: The global nitrogen cycle in the
708 Twentyfirst century, *Philosophical Transactions of the Royal Society B: Biological Sciences*,
709 368, <https://doi.org/10.1098/rstb.2013.0164>, 2013.
- 710 Girach, I. A., Tripathi, N., Nair, P. R., Sahu, L. K., and Ojha, N.: O₃ and CO in the South Asian
711 outflow over the Bay of Bengal: Impact of monsoonal dynamics and chemistry, *Atmos Environ*,
712 233, <https://doi.org/10.1016/j.atmosenv.2020.117610>, 2020.
- 713 Griffiths, P. T., Murray, L. T., Zeng, G., Shin, Y. M., Abraham, N. L., Archibald, A. T., Deushi,
714 M., Emmons, L. K., Galbally, I. E., Hassler, B., Horowitz, L. W., Keeble, J., Liu, J., Moeini,



- 715 O., Naik, V., and Connor, F. M. O.: Tropospheric ozone in CMIP6 simulations, 4187–4218,
716 2021.
- 717 Grigas, T., Ovadnevaite, J., Ceburnis, D., Moran, E., McGovern, F. M., Jennings, S. G., and
718 O’Dowd, C.: Sophisticated Clean Air Strategies Required to Mitigate Against Particulate
719 Organic Pollution, *Sci Rep*, 7, <https://doi.org/10.1038/srep44737>, 2017.
- 720 Guerreiro, C. B. B., Foltescu, V., and de Leeuw, F.: Air quality status and trends in Europe,
721 *Atmos Environ*, 98, 376–384, <https://doi.org/10.1016/j.atmosenv.2014.09.017>, 2014.
- 722 IPCC, Masson-Delmotte, V., Zhai, P., Chen, Y., Goldfarb, L., Gomis, M. I., Matthews, J. B. R.,
723 Berger, S., Huang, M., Yelekçi, O., Yu, R., Zhou, B., Lonnoy, E., Maycock, T. K., Waterfield,
724 T., Leitzell, K., & Caud, N. Working Group I Contribution to the Sixth Assessment Report of
725 the Intergovernmental Panel on Climate Change Edited by. www.ipcc.ch, 2021.
- 726 Jacobson, M. Z.: *Atmospheric Pollution: History, Science, and Regulation*, Cambridge
727 University Press, Cambridge, 2002.
- 728 Jeon, W. B., Lee, S. H., Lee, H., Park, C., Kim, D. H., and Park, S. Y.: A study on high ozone
729 formation mechanism associated with change of NO_x/VOCs ratio at a rural area in the Korean
730 Peninsula, *Atmos Environ*, 89, 10–21, <https://doi.org/10.1016/j.atmosenv.2014.02.005>, 2014.
- 731 Jonson, J. E., Stohl, A., Fiore, A. M., Hess, P., Szopa, S., Wild, O., Zeng, G., Dentener, F. J.,
732 Lupu, A., Schultz, M. G., Duncan, B. N., Sudo, K., Wind, P., Schulz, M., Marmer, E., Cuvelier,
733 C., Keating, T., Zuber, A., Valdebenito, A., Dorokhov, V., De Backer, H., Davies, J., Chen, G.
734 H., Johnson, B., Tarasick, D. W., Stübi, R., Newchurch, M. J., Von Der Gathen, P., Steinbrecht,
735 W., and Claude, H.: A multi-model analysis of vertical ozone profiles, *Atmos Chem Phys*, 10,
736 5759–5783, <https://doi.org/10.5194/acp-10-5759-2010>, 2010.



- 737 Khiem, M., Ooka, R., Huang, H., Hayami, H., Yoshikado, H., and Kawamoto, Y.: Analysis of
738 the Relationship between Changes in Meteorological Conditions and the Variation in Summer
739 Ozone Levels over the Central Kanto Area, *Advances in Meteorology*, 2010, 1–13,
740 <https://doi.org/10.1155/2010/349248>, 2010.
- 741 Lamarque, J. F. and Solomon, S.: Impact of changes in climate and halocarbons on recent lower
742 stratosphere ozone and temperature trends, *J Clim*, 23, 2599–2611,
743 <https://doi.org/10.1175/2010JCLI3179.1>, 2010.
- 744 Lamarque, J. F., Kinnison, D. E., Hess, P. G., and Vitt, F. M.: Simulated lower stratospheric
745 trends between 1970 and 2005: Identifying the role of climate and composition changes,
746 *Journal of Geophysical Research Atmospheres*, 113, <https://doi.org/10.1029/2007JD009277>,
747 2008.
- 748 Lamarque, J. F., Bond, T. C., Eyring, V., Granier, C., Heil, A., Klimont, Z., Lee, D., Liousse,
749 C., Mieville, A., Owen, B., Schultz, M. G., Shindell, D., Smith, S. J., Stehfest, E., Van
750 Aardenne, J., Cooper, O. R., Kainuma, M., Mahowald, N., McConnell, J. R., Naik, V., Riahi,
751 K., and Van Vuuren, D. P.: Historical (1850–2000) gridded anthropogenic and biomass burning
752 emissions of reactive gases and aerosols: Methodology and application, *Atmos Chem Phys*, 10,
753 7017–7039, <https://doi.org/10.5194/acp-10-7017-2010>, 2010.
- 754 Lamarque, J. F., Emmons, L. K., Hess, P. G., Kinnison, D. E., Tilmes, S., Vitt, F., Heald, C. L.,
755 Holland, E. A., Lauritzen, P. H., Neu, J., Orlando, J. J., Rasch, P. J., and Tyndall, G. K.: CAM-
756 chem: Description and evaluation of interactive atmospheric chemistry in the Community Earth
757 System Model, *Geosci Model Dev*, 5, 369–411, <https://doi.org/10.5194/gmd-5-369-2012>,
758 2012.
- 759 Lefohn, A. S., Malley, C. S., Smith, L., Wells, B., Hazucha, M., Simon, H., Naik, V., Mills, G.,
760 Schultz, M. G., Paoletti, E., De Marco, A., Xu, X., Zhang, L., Wang, T., Neufeld, H. S.,



761 Musselman, R. C., Tarasick, D., Brauer, M., Feng, Z., Tang, H., Kobayashi, K., Sicard, P.,
762 Solberg, S., and Gerosa, G.: Tropospheric ozone assessment report: Global ozone metrics for
763 climate change, human health, and crop/ecosystem research, *Elementa*, 6,
764 <https://doi.org/10.1525/elementa.279>, 2018.

765 Lin, M., Fiore, A. M., Cooper, O. R., Horowitz, L. W., Langford, A. O., Levy, H., Johnson, B.
766 J., Naik, V., Oltmans, S. J., and Senff, C. J.: Springtime high surface ozone events over the
767 western United States: Quantifying the role of stratospheric intrusions, *Journal of Geophysical*
768 *Research Atmospheres*, 117, <https://doi.org/10.1029/2012JD018151>, 2012.

769 Lupaşcu, A., Otero, N., Minkos, A., and Butler, T.: Attribution of surface ozone to NO_x and
770 volatile organic compound sources during two different high ozone events, *Atmos Chem Phys*,
771 22, 11675–11699, <https://doi.org/10.5194/acp-22-11675-2022>, 2022.

772 Masson-Delmotte, V., Zhai, P., Chen, Y., Goldfarb, L., Gomis, M. I., Matthews, J. B. R., Berger,
773 S., Huang, M., Yelekçi, O., Yu, R., Zhou, B., Lonnoy, E., Maycock, T. K., Waterfield, T.,
774 Leitzell, K., and Caud, N.: Working Group I Contribution to the Sixth Assessment Report of
775 the Intergovernmental Panel on Climate Change Edited by, 2021.

776 McVeigh, P., O'Dowd, C., and Berresheim, H.: Eddy Correlation Measurements of Ozone
777 Fluxes over Coastal Waters West of Ireland, *Advances in Meteorology*, 2010,
778 <https://doi.org/10.1155/2010/754941>, 2010.

779 Moiseenko, K. B., Vasileva, A. V., Skorokhod, A. I., Belikov, I. B., Repin, A. Y., and Shtabkin,
780 Y. A.: Regional Impact of Ozone Precursor Emissions on NO_x and O₃ Levels at ZOTTO Tall
781 Tower in Central Siberia, *Earth and Space Science*, 8, <https://doi.org/10.1029/2021EA001762>,
782 2021.



783 Molod, A., Takacs, L., Suarez, M., and Bacmeister, J.: Development of the GEOS-5
784 atmospheric general circulation model: Evolution from MERRA to MERRA2, *Geosci Model*
785 *Dev*, 8, 1339–1356, <https://doi.org/10.5194/gmd-8-1339-2015>, 2015.

786 Monks, P. S., Archibald, A. T., Colette, A., Cooper, O., Coyle, M., Derwent, R., Fowler, D.,
787 Granier, C., Law, K. S., Mills, G. E., Stevenson, D. S., Tarasova, O., Thouret, V., Von
788 Schneidmesser, E., Sommariva, R., Wild, O., and Williams, M. L.: Tropospheric ozone and
789 its precursors from the urban to the global scale from air quality to short-lived climate forcer,
790 <https://doi.org/10.5194/acp-15-8889-2015>, 13 August 2015.

791 Nalam, A., Lupascu, A., Ansari, T., and Butler, T.: Regional and sectoral contributions of NO_x
792 and reactive carbon emission sources to global trends in tropospheric ozone during the 2000–
793 2018 period, <https://doi.org/10.5194/egusphere-2024-432>, 12 March 2024.

794 O’Dowd, C., Ceburnis, D., Ovadnevaite, J., Vaishya, A., Rinaldi, M., and Facchini, M. C.: Do
795 anthropogenic, continental or coastal aerosol sources impact on a marine aerosol signature at
796 Mace Head?, *Atmos Chem Phys*, 14, 10687–10704, [https://doi.org/10.5194/acp-14-10687-](https://doi.org/10.5194/acp-14-10687-2014)
797 2014, 2014.

798 Oltmans, S. J., Lefohn, A. S., Shadwick, D., Harris, J. M., Scheel, H. E., Galbally, I., Tarasick,
799 D. W., Johnson, B. J., Brunke, E. G., Claude, H., Zeng, G., Nichol, S., Schmidlin, F., Davies,
800 J., Cuevas, E., Redondas, A., Naoe, H., Nakano, T., and Kawasato, T.: Recent tropospheric
801 ozone changes - A pattern dominated by slow or no growth, *Atmos Environ*, 67, 331–351,
802 <https://doi.org/10.1016/j.atmosenv.2012.10.057>, 2013.

803 Pall E E, E. and Butler, C. J.: Comparison of sunshine records and synoptic cloud observations:
804 a case study for Ireland, n.d.



- 805 Pan, C., Zhu, B., Gao, J., Hou, X., Kang, H., and Wang, D.: Quantifying Arctic lower
806 stratospheric ozone sources in winter and spring, *Sci Rep*, 8, [https://doi.org/10.1038/s41598-](https://doi.org/10.1038/s41598-018-27045-5)
807 018-27045-5, 2018.
- 808 Paoletti, E.: Impact of ozone on Mediterranean forests: A review, *Environmental Pollution*,
809 144, 463–474, <https://doi.org/10.1016/j.envpol.2005.12.051>, 2006.
- 810 Parrish, D. D., Derwent, R. G., Steinbrecht, W., Stübi, R., Van Malderen, R., Steinbacher, M.,
811 Trickl, T., Ries, L., & Xu, X.: Zonal Similarity of Long-Term Changes and Seasonal Cycles of
812 Baseline Ozone at Northern Midlatitudes. *Journal of Geophysical Research: Atmospheres*,
813 125(13), 1–19. <https://doi.org/10.1029/2019JD031908>, 2020.
- 814 Pausata, F. S. R., Pozzoli, L., Vignati, E., & Dentener, F. J.: North Atlantic Oscillation and
815 tropospheric ozone variability in Europe: Model analysis and measurements intercomparison.
816 *Atmospheric Chemistry and Physics*, 12(14), 6357–6376. [https://doi.org/10.5194/acp-12-](https://doi.org/10.5194/acp-12-6357-2012)
817 6357-2012, 2012.
- 818 Pio, C. A., Feliciano, M. S., Vermeulen, A. T., and Sousa, E. C.: Seasonal variability of ozone
819 dry deposition under southern European climate conditions, in Portugal, *Atmospheric*
820 *Environment*, 195–205 pp., 2000.
- 821 Russo, M. R., Kerridge, B. J., Abraham, N. L., Keeble, J., Latter, B. G., Siddans, R., Weber, J.,
822 Griffiths, P. T., Pyle, J. A., and Archibald, A. T.: Seasonal , interannual and decadal variability
823 of tropospheric ozone in the North Atlantic : comparison of UM-UKCA and remote sensing
824 observations for 2005 – 2018, 6169–6196, 2023.
- 825 Shindell, D. T., Chin, M., Dentener, F., Doherty, R. M., Faluvegi, G., Fiore, A. M., Hess, P.,
826 Koch, D. M., Mackenzie, I. A., Sanderson, M. G., Schultz, M. G., Schulz, M., Stevenson, D.
827 S., Teich, H., Textor, C., Wild, O., Bergmann, D. J., Bey, I., Bian, H., Cuvelier, C., Duncan, B.
828 N., Folberth, G., Horowitz, L. W., Jonson, J., Kaminski, J. W., Marmer, E., Park, R., Pringle,



- 829 K. J., Schroeder, S., Szopa, S., Takemura, T., Zeng, G., Keating, T. J., and Zuber, A.:
830 Atmospheric Chemistry and Physics A multi-model assessment of pollution transport to the
831 Arctic, *Atmos. Chem. Phys.*, 5353–5372 pp., 2008.
- 832 Sicard, P., Serra, R., and Rossello, P.: Spatiotemporal trends in ground-level ozone
833 concentrations and metrics in France over the time period 1999-2012, *Environ Res.*, 149, 122–
834 144, <https://doi.org/10.1016/j.envres.2016.05.014>, 2016.
- 835 Simmonds, P. G., Derwent, R. G., Manning, A. L., and Spain, G.: Significant growth in surface
836 ozone at Mace Head, Ireland, 1987-2003, *Atmos Environ.*, 38, 4769–4778,
837 <https://doi.org/10.1016/j.atmosenv.2004.04.036>, 2004.
- 838 Soares, J., UBA, D. P., UBA, S. K., EEA, A. G. O., EEA, A. G., & Horálek, J. Health Risk
839 Assessment of Air Pollution: assessing the environmental burden of disease in Europe in 2021.
840 ETC HE Report, 7, 104, 2021.
- 841 Spohn, T. K., Martin, D., Geever, M., and O'Dowd, C.: Effect of COVID-19 lockdown on
842 regional pollution in Ireland, *Air Qual Atmos Health*, 15, 221–234,
843 <https://doi.org/10.1007/s11869-021-01098-4>, 2022.
- 844 Seinfeld, J. H. and Pandis, S. N.: *Atmospheric Chemistry and Physics: From Air Pollution to*
845 *Climate Change*, Wiley-VCH, New York, 1997.
- 846 Seinfeld, J. H. and Pandis, S. N.: *Atmospheric Chemistry and Physics: From Air Pollution to*
847 *Climate Change*, 3rd edn., Wiley, Hoboken, NJ, 2016.
- 848 Stunder, B.J.B.: Global Data Assimilation System (GDAS) Archive Information, NOAA Air
849 Resources Laboratory, Silver Spring, MD, USA, December 1, 2004
- 850 Tafidis, P., Gholamnia, M., Sajadi, P., Krishnan Vijayakrishnan, S., and Pilla, F.: Evaluating the
851 impact of urban traffic patterns on air pollution emissions in Dublin: a regression model using



852 google project air view data and traffic data, European Transport Research Review, 16,
853 <https://doi.org/10.1186/s12544-024-00671-z>, 2024.

854 Tan, J., Fu, J. S., Dentener, F., Sun, J., Emmons, L., Tilmes, S., Flemming, J., Takemura, T.,
855 Bian, H., Zhu, Q., Yang, C. E., and Keating, T.: Source contributions to sulfur and nitrogen
856 deposition - An HTAP II multi-model study on hemispheric transport, Atmos Chem Phys, 18,
857 12223–12240, <https://doi.org/10.5194/acp-18-12223-2018>, 2018.

858 Tavella, R. A. and da Silva Júnior, F. M. R.: Watch out for trends: did ozone increased or
859 decreased during the COVID-19 pandemic?, Environmental Science and Pollution Research,
860 28, 67880–67885, <https://doi.org/10.1007/s11356-021-17142-w>, 2021.

861 Tilmes, S., Sanderson, B. M., and O'Neill, B. C.: Climate impacts of geoengineering in a
862 delayed mitigation scenario, Geophys Res Lett, 43, 8222–8229,
863 <https://doi.org/10.1002/2016GL070122>, 2016.

864 Tilmes, S., Lamarque, J. F., Emmons, L. K., Kinnison, D. E., Ma, P. L., Liu, X., Ghan, S.,
865 Bardeen, C., Arnold, S., Deeter, M., Vitt, F., Ryerson, T., Elkins, J. W., Moore, F., Spackman,
866 J. R., and Val Martin, M.: Description and evaluation of tropospheric chemistry and aerosols
867 in the Community Earth System Model (CESM1.2), Geosci Model Dev, 8, 1395–1426,
868 <https://doi.org/10.5194/gmd-8-1395-2015>, 2015.

869 Todorović, M. N., Radenković, M. B., Rajšić, S. F., & Ignjatović, L. M. Evaluation of mortality
870 attributed to air pollution in the three most populated cities in Serbia. International Journal of
871 Environmental Science and Technology, 16(11), 7059–7070. [https://doi.org/10.1007/s13762-](https://doi.org/10.1007/s13762-019-02384-6)
872 019-02384-6, 2019.

873 Tripathi, O. P., Jennings, S. G., O'Dowd, C. D., Coleman, L., Leinert, S., O'Leary, B., Moran,
874 E., O'Doherty, S. J., and Spain, T. G.: Statistical analysis of eight surface ozone measurement



- 875 series for various sites in Ireland, *Journal of Geophysical Research Atmospheres*, 115, 1–20,
876 <https://doi.org/10.1029/2010JD014040>, 2010.
- 877 Tripathi, O. P., Jennings, S. G., O’Dowd, C., O’Leary, B., Lambkin, K., Moran, E., O’Doherty,
878 S. J., and Gerard Spain, T.: An assessment of the surface ozone trend in Ireland relevant to air
879 pollution and environmental protection, *Atmos Pollut Res*, 3, 341–351,
880 <https://doi.org/10.5094/APR.2012.038>, 2012.
- 881 Tripathi, O. P., Jennings, S. G., Colman, L., Lambkin, K., Moran, E., and Dowd, C. O.: Ozone
882 levels , changes and trends over Ireland – an Integrated Analysis, 2013.
- 883 Tripathi, O. P., Gerard Jennings, S., Colman, L., Lambkin, K., and Moran, E.: EPA STRIVE
884 Programme 2007-2013 Ozone levels, changes and trends over Ireland-an Integrated Analysis
885 (2006-AQ-MS-50) STRIVE Report, n.d.
- 886 Tripathi, R. M., Vinod Kumar, A., Manikandan, S. T., Bhalke, S., Mahadevan, T. N., and
887 Puranik, V. D.: Vertical distribution of atmospheric trace metals and their sources at Mumbai,
888 India, *Atmos Environ*, 38, 135–146, <https://doi.org/10.1016/j.atmosenv.2003.09.006>, 2004.
- 889 Vautard, R., Moran, M. D., Solazzo, E., Gilliam, R. C., Matthias, V., Bianconi, R., Chemel, C.,
890 Ferreira, J., Geyer, B., Hansen, A. B., Jericevic, A., Prank, M., Segers, A., Silver, J. D.,
891 Werhahn, J., Wolke, R., Rao, S. T., and Galmarini, S.: Evaluation of the meteorological forcing
892 used for the Air Quality Model Evaluation International Initiative (AQMEII) air quality
893 simulations, *Atmos Environ*, 53, 15–37, <https://doi.org/10.1016/j.atmosenv.2011.10.065>, 2012.
- 894 Van Der Werf, G. R., Randerson, J. T., Giglio, L., Collatz, G. J., Mu, M., Kasibhatla, P. S.,
895 Morton, D. C., Defries, R. S., Jin, Y., and Van Leeuwen, T. T.: Global fire emissions and the
896 contribution of deforestation, savanna, forest, agricultural, and peat fires (1997-2009), *Atmos*
897 *Chem Phys*, 10, 11707–11735, <https://doi.org/10.5194/acp-10-11707-2010>, 2010.



- 898 Wespes, C., Hurtmans, D., Clerbaux, C., and Coheur, P. F.: O₃ variability in the troposphere as
899 observed by IASI over 2008-2016: Contribution of atmospheric chemistry and dynamics, *J*
900 *Geophys Res*, 122, 2429–2451, <https://doi.org/10.1002/2016JD025875>, 2017.
- 901 WHO. Global Air Quality Guidelines: Particulate Matter (PM_{2.5} and PM₁₀), Ozone, Nitrogen
902 Dioxide, Sulfur Dioxide and Carbon Monoxide (World Health Organization, 2021).
- 903 Yerramilli, A., Srinivas Challa, V., Rao Dodla, V. B., Myles, L. T., Pendergrass, W. R., Vogel,
904 C. A., Tuluri, F., Baham, J. M., Hughes, R., Patrick, C., Young, J., & Swanier, S. Simulation of
905 surface ozone pollution in the Central Gulf Coast region during summer synoptic condition
906 using WRF/Chem air quality model. *Atmospheric Pollution Research*, 3(1), 55–71.
907 <https://doi.org/10.5094/APR.2012.005>, 2012.
- 908 Young, P. J., Archibald, A. T., Bowman, K. W., Lamarque, J., Naik, V., Stevenson, D. S., and
909 Tilmes, S.: Pre-industrial to end 21st century projections of tropospheric ozone from the
910 Atmospheric Chemistry and Climate Model Intercomparison Project (ACCMIP), 2063–2090,
911 <https://doi.org/10.5194/acp-13-2063-2013>, 2013.
- 912 Zhang, J. J., Wei, Y., & Fang, Z. Ozone pollution: A major health hazard worldwide. *Frontiers*
913 *in Immunology*, 10(OCT), 1–10. <https://doi.org/10.3389/fimmu.2019.02518>, 2019.
- 914 Zhu, T., Melamed, M., Parrish, D., Gauss, M., Klenner, L. G., Lawrence, M., Konare, A., and
915 Liousse, C.: Impacts of Megacities on Air Pollution and Climate, WMO, Geneva, 2012.
- 916
- 917
- 918
- 919



920

921 **Figure Captions**

922 **Figure 1.** The map of EPA O₃ measurement sites over Ireland with classification of
923 backgrounds.

924 **Figure 2.** Annual average O₃ concentration at different sites in Ireland. In each box, the
925 lowest whisker level represents the 5th percentile, the box spans from the 25th to the 75th
926 percentile, the horizontal line within the box represents the median 50th percentile, and the
927 upper whisker represents the 95th percentile. The average of monthly O₃ values calculated for
928 the entire period of each station, and the red line shows the average monthly O₃ variation of
929 all sites top axis shows the month (1– 12).

930 **Figure 3.** Monthly trend analysis of O₃ at different sites for 10 year period. (2012-2022)
931 Adopting the trend reliability scale defined for TOAR-II studies (Chang et al., 2023), trends
932 with very high certainty are marked by ***($p \leq 0.001$), , trends with high certainty with **(p
933 ≤ 0.01), and low to medium certainty with *($p \leq 0.05$). Positive trends are in red shade and
934 negative trends are in blue shade.

935 **Figure 5.-** Trend in O₃ precursors NO₂ (a), and CH₄ (b) at different sites. Trends with very
936 high certainty are marked by ***($p \leq 0.001$), , trends with high certainty with **($p \leq 0.01$),,
937 and low to medium certainty with *($p \leq 0.05$).

938 **Figure 6.** Percentage change in NO₂ and O₃ during the lockdown period of 2020 as
939 compared to the 2017-2019 average at different sites in Ireland for (a) March (b) April (c)
940 May Month.

941 **Figure 7.** The comparison of Monthly CAM4 – Chem O₃ and Monthly O₃ observations at
942 five sites in Ireland.



943 **Figure 8.** Absolute contribution of major NO_x sources (a) (NO_x Tagging) and VOC source
944 (b) (NO_x Tagging) to the CAM4-Chem simulated surface O₃ for the Mace Head grid cell
945 between 2000-2018.

946 **Figure 9.** Trends in contributions to monthly average modelled Mace Head grid cell surface
947 O₃ at for the 2000-2018 period derived from (a) NO_x tagging and (b) VOC tagging.

948 **Figure 10.** Trend in seasonal Average of observed O₃ (black) and Model O₃ (red) at Mace
949 head, separated into clean sector and EU-influenced sector.

950 **Figure 11.** Exceedances measured at Mace Head per month from 2000 until 2022, during the
951 clean air sector (green) and EU influenced sector (yellow). The percentage of both to total
952 exceedances is shown in the inlay.

953 **Figure 12.** (a) The trend in Spring-time exceedances measured at Mace Head between 2000
954 and 2022 (blue) with the clean-air exceedances (gold), and (b) The trend in 95th percentile
955 of spring (Mar- May) O₃ measured in µg /m³ for the clean sector (blue) and the EU-
956 influenced sector (gold).

957 **Figure 13** Monthly cumulative Mace Head grid cell O₃ contributions to EU influenced
958 sector and clean sector exceedances (a) NO_x tagging and (b) VOC tagging Mace Head grid
959 cell.

960

961

962

963

964